July 2021

LYAPUNOV FUNCTION-BASED STABILIZING CONTROL SCHEME FOR WIRELESS POWER TRANSFER SYSTEMS WITH LCC COMPENSATION NETWORK

Abu Shahir Md Khalid Hasan
Louisiana State University and Agricultural and Mechanical College

LYAPUNOV FUNCTION-BASED STABILIZING CONTROL SCHEME FOR WIRELESS POWER TRANSFER SYSTEMS WITH LCC COMPENSATION NETWORK

A Thesis

Submitted to the Graduate Faculty of the
Louisiana State University and
Agriculture and Mechanical College
in partial fulfillment of the
requirements for the degree of
Master of Science

in

The Department of Electrical and Computer Engineering

by
Abu Shahir Md Khalid Hasan
M.Sc., Electrical and Electronic Engineering
Bangladesh University of Engineering and Technology, Bangladesh 2019
August 2021

To my family and friends who helped in different ways

Acknowledgment

I take pleasure in submitting herewith the report on “LYAPUNOV FUNCTION-BASED STABILIZING CONTROL SCHEME FOR WIRELESS POWER TRANSFER SYSTEMS WITH LCC COMPENSATION NETWORK” in partial fulfillment of the requirements for the degree of Master of Science in Electrical and Computer Engineering.

Dr. Mehdi Farasat, my adviser, has been a huge help to me in every aspect. Dr. Farasat provided me with a wealth of knowledge, and his words of wisdom assisted me in making many of my thesis and life decisions. His willingness and support ensured the research's success, and his advice on how to communicate the findings to society allowed the initiative to be fine-tuned. He was tolerant with my inexcusable errors and flaws, and I am grateful for that.

I would also like to express my gratitude to Dr. Shahab Mehraeen and Dr. Amin Kargarian, who graciously agreed to serve on my thesis committee. They were not only my committee members, but also my instructors in fascinating courses.

There were times when life was difficult for me, but my family stood by me. They showed me the way to healing and rebirth, and I will never be able to express my thanks to them. Because I would not be who I am now if it were not for them. I also want to thank my instructors for teaching me not only about the courses, but also about life. I would also like to express my gratitude to Baton Rouge's Bangladeshi student community for their unwavering support.

Table Of Contents

Abstract

A stabilizing control scheme based on a Lyapunov function is proposed for wireless power transfer (or WPT) systems. A state-space model of the WPT system is developed and the Lyapunov function is formulated based on an energy equation of the system involving state variables. The internal resistance of a battery varies during charge and discharge. Therefore, if a WPT system is used to charge a battery, its output load will vary. Furthermore, the coupling coefficient between the transmitter (primary) and receiver (secondary) coils decreases when they are misaligned. Comparative case studies are conducted to verify the efficacy of the proposed controller in maintaining stability of the WPT system under load variation and acute misalignment of transmitter and receiver coils.

Introduction

The concerns of fossil fuel depletion and global warming, as well as newly enacted CO2 emission limitations, are among the key causes driving society and governments to adopt plug-in hybrid electric vehicles (PHEV) and electric cars (EV) in the transportation system. The automobile industry is facing rising demand, with electric vehicle sales estimated to reach 5.9 million units by 2020. Providing convenient and safe battery charging is one of the issues in the development of PHEVs and EVs. There are two types of EV battery charging methods: wired (conductive) and wireless charging.

The user connects a cable from the power outlet or charging station to the EV in the wired charging method. Handling large gauge cable makes wired charging inconvenient, and it can even be dangerous owing to tripping hazards, especially in wet weather. Wireless charging has some intrinsic advantages over cable charging, such as safety, convenience, reliability, and weather resistance [1, 2].

Nikola Tesla proposed the concept of wireless energy transmission in 1899. Wireless power transfer (WPT) technology has been investigated and deployed for a variety of applications over the last few decades, including biomedical implants [3], induction heating [4], mobile battery chargers [5], E-bikes [6], electric vehicles [7], electric buses [8], and trains [9].

There are two types of WPT technologies: far field electromagnetic and near field electromagnetic. Far field radiation, such as microwave and laser, uses radio frequency and may transmit relatively modest power (for safety reasons) over many meters [10]. Near field (non-radiative) electromagnetic coupling, such as inductive coupling, capacitive coupling, and magnetic coupling, on the other hand, operates at a frequency of tens to hundreds of kHz. Transferred power in near

field WPTs can be in the tens of kW range, with a transfer distance of only a few millimeters [11]. Inductive and magnetic coupling are extensively utilized near field WPT technologies because to their simplicity and high efficiency [12]. One coil in the transmitter (also known as primary side) creates an alternating electromagnetic field, while another coil in the receiver (secondary side) receives the supplied power in both methods. Magnetic coupled WPT is actually no different from inductive coupled WPT, which has been investigated for many years [13], except for the higher frequency and the usage of ferrite.

Magnetic linked WPT systems can be classified as distributed or lumped topologies in general. A transmitter coil creating a lengthy track and receiver coil(s) linked to a tiny piece of the transmitter coil make up a distributed system. The distributed system is made to transfer power in a continuous manner. When the coils are aligned, the lumped system can transfer power since it consists of two discrete coils at the transmitter and receiver set in a fixed position. Closely coupled and loosely coupled systems are two types of lumped systems. The user must plug in the primary [14, 15] in a closely coupled lumped system because the air gaps between coils are relatively narrow. The air gap in a loosely coupled lumped system is vast and does not require human involvement.

In this report, a Lyapunov based controller is compared with PI controller for loosely coupled lumped WPT systems for EVs and PHEVs. The fundamentals of magnetic coupled WPT are covered in the second section. The state of the art of WPT is discussed in the third section. In fourth section, fundamentals of Lyapunov based controller for SLCC and PLCC Compensation Network based WPT System are presented. In fourth section, the stability of Lyapunov Controller is investigated using the variable resistance model as well as a comparison between Lyapunov based controller and PI controller for the WPT system is presented.

Fundamentals of WPT

A typical block diagram of a WPT system is shown in Figure 1. A wireless charger and a conventional charger both work on the same basic premise. The charger is plugged into an electrical outlet. After that, an AC to DC converter with power factor correction (PFC) rectifies the AC voltage.

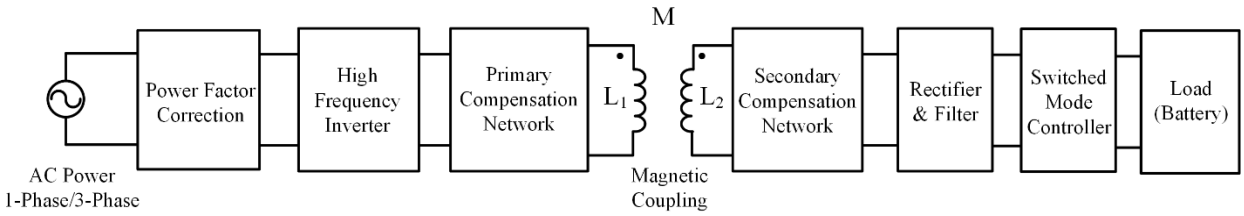

Figure 1. WPT system structure

After that, DC power is converted to AC using a high frequency (HF) DC to AC converter (inverter). In a wired charger, the following stage is an isolated transformer, whereas in a WPT charger, the next stage is a series of loosely connected coils. An HF transformer may be required for WPT applications to provide electrical isolation of the WPT primary coupler and cable from the utility. An HF rectifier and filter are located on the secondary side. A switched mode controller may also be used before the load to increase the power transmission capability.

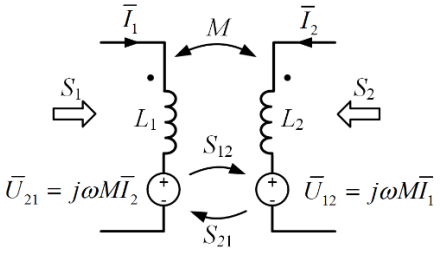

Figure 2. Two-coil WPT model

Figure 2 should be considered to get a better understanding of the distinction between strongly and loosely connected coils. L_1 and L_2 are the self-inductances of the primary and secondary coils, respectively, in this diagram. I_1 and I_2 are the currents in the two coils, respectively. Induced voltage in the primary and secondary coils is represented by U_{12} and U_{21}, respectively. S_1 and S_2 represent the apparent power entering the primary and secondary coils, respectively. S_{12} and S_{21} represent the power exchanged between the primary and secondary coils, and they are computed as follows [13]

$$\bar{S}_{12} = -\bar{U}_{12}\bar{I}_2^* = -j\omega M\bar{I}_1\bar{I}_2^* = \omega M I_1 I_2 \sin\varphi_{12} - j\omega M I_1 I_2 \cos\varphi_{12} \quad (1)$$

$$\bar{S}_{21} = -\bar{U}_{21}\bar{I}_1^* = -j\omega M\bar{I}_2\bar{I}_1^* = -\omega M I_1 I_2 \sin\varphi_{12} - j\omega M I_1 I_2 \cos\varphi_{12} \quad (2)$$

The phase difference between $\bar{I}_1$ and $\bar{I}_2$ is φ_{12} in this case. The active power transferred from the primary coil to the secondary coil can be expressed in the following way:

$$P_{12} = \omega M I_1 I_2 \sin\varphi_{12} \quad (3)$$

For $\varphi_{12}=\pi/2$, the maximum active power is transferred. In the two-coil arrangement, total reactive power can be represented as

$$Q = \omega(L_1 I_1^2 + L_2 I_2^2 + 2M I_1 I_2 \cos\varphi_{12}) \quad (4)$$

Higher reactive power translates to higher magnetizing power, which might result in more copper and core losses. The active to reactive power ratio should be maximized to optimize transfer efficiency. The following is how this ratio is defined [13]

$$\frac{P_{12}}{Q} = \frac{\omega M I_1 I_2 \sin\varphi_{12}}{\omega(L_1 I_1^2 + L_2 I_2^2 + 2M I_1 I_2 \cos\varphi_{12})} = \frac{k\sqrt{1-(\cos\varphi_{12})^2}}{x + \frac{1}{x} + 2k\cos\varphi_{12}} \quad (5)$$

where

$$k = \frac{M}{\sqrt{L_1 L_2}} \quad (6)$$

$$x = \sqrt{\frac{L_1}{L_2}}\frac{I_1}{I_2} \quad (7)$$

The coupling coefficient, abbreviated as *k*, is a helpful metric for comparing the magnetic properties of different coupler topologies; it is the fraction of magnetic flux produced by one coil and linked to the opposite one [16].

The following equation must be satisfied to get the optimum active to reactive power ratio:

$$\cos\varphi_{12} = -\frac{2k}{x + \frac{1}{x}} \quad (8)$$

k is close to 1 in strongly linked coils, and because I_2 is induced current by I_1, *x* will be close to 1 (if L_1=L_2). As a result, cosφ_{12}≈-1 gives φ_{12}≈180°. Because *k* is near to 0 in loosely linked coils, φ_{12} is around 90 degrees [13].

In the case of loosely connected WPTs with *k*<0.5, a compensation network is frequently added to both the primary and secondary sides, with the goal of maximizing power transfer. According to (3), φ_{12} must be equal to 90° in order to fulfill this goal, and this is independent of the *k* value. This means I_2 should be 90 degrees behind I_1. U_{12} will be in phase with I_2 in this situation. As a result, the impedance seen from U_{12} at the operating frequency will be pure resistive. As a result, the

secondary compensation network is meant to attain a φ_{12} close to 90° and minimize the coils VA. As a result, the losses in the coils will be reduced. The primary compensation network, on the other hand, is designed to cancel reactive power and, as a result, reduce the VA of the power electronics converter, resulting in losses.

Literature Review

Compensation Networks

Compensation networks are used on both the primary and secondary levels in WPT applications. The primary goal of implementing a compensation network on the primary side is to reduce the VA and losses of the switching power supply. The secondary compensation network is meant to boost the secondary coil's short-circuit current and hence improve power transfer performance [17].

Mutual inductance is low when there is a big air gap between the main and secondary. As a result, the magnetizing current is extremely high. When the air gap widens or a misalignment occurs, the situation gets worse. Leakage inductance is substantially more than mutual inductance in this situation. As a result, the coil suffers from a high circulating current and, as a result, a loss. The imaginary part of the input impedance must be reduced to reduce circulating current and hence losses. A compensation network [18] is used to do this.

Figure 3 depicts four fundamental compensation networks: series-series (SS), series-parallel (SP), parallel-series (PS), and parallel-parallel (PP). The position of the capacitor in relation to the inductances of the coils is used to designate these networks. A common way is to choose a secondary capacitor that resonates with the secondary coil's self-inductance. However, the primary capacitance is intended to compensate for both the primary coil self-inductance and the reflected imaginary impedance. The secondary resonant frequency is set equal to the zero-phase angle frequency of the impedance observed from the source [13].

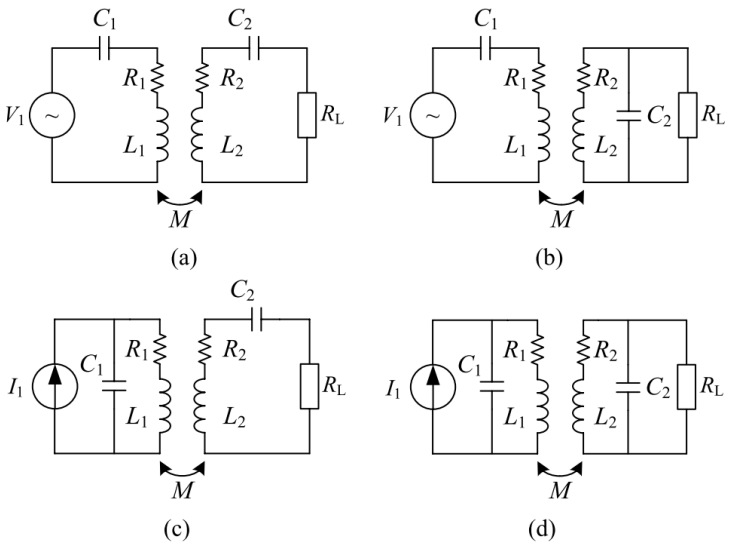

Figure 3. Four common compensation topologies (a) SS (b) SP (c) PS (d) PP [13]

When there is series and parallel compensation in the secondary, Table 1 summarizes the reflected resistance and reactance. The reflected impedance from the secondary to the primary is denoted by Z_r in this diagram. As can be seen, the imaginary part of the reflected impedance for a series-compensated secondary is zero, whereas a capacitive load is reflected by a parallel-compensated secondary. This is a significant distinction between parallel-compensated secondary and series secondary [19].

Table 1. Reflected impedance for series and parallel-compensated secondary

Serious Secondary	$Re(Z_r) = \frac{\omega_0^2 M^2}{R}$	$Im(Z_r) = 0$
Parallel Secondary	$Re(Z_r) = \frac{M^2 R}{L_2^2}$	$Im(Z_r) = -\frac{\omega_0 M^2}{L_2}$

Table 2. Conventional primary capacitor design for four basic compensation networks

SS	$C_1 = \frac{1}{\omega_0^2 L_1}$

SP	$C_1 = \frac{1}{\omega_0^2(L_1 - M^2/L_2)}$
PS	$C_1 = \frac{L_1 - M^2/L_2}{(RM^2/L_2^2)^2 + \omega_0^2(L_1 - M^2/L_2)^2}$
PP	$C_1 = \frac{L_1}{(\omega_0^2 M^2/R)^2 + \omega_0^2 L_1^2}$

Table 2 shows a popular method for designing primary capacitance for four basic compensation networks. As can be shown, the needed primary compensation capacitance for SS topologies is independent of mutual inductance and load, whereas capacitance for SP topologies is dependent on mutual inductance. Furthermore, the needed primary compensation capacitance for parallel-compensated primary is a function of both the mutual inductance and the load. As a result, for parallel-compensated primary, the primary compensation capacitance must be designed for the needed power [19].

Z_{in}, the impedance measured from the power source, can be expressed as follows:

$$Z_{in} = \begin{cases} \frac{1}{j\omega C_1} + j\omega L_1 + Z_r & \text{Series-compensated primary} \\ \frac{1}{j\omega C_1 + \frac{1}{j\omega L_1 + Z_r}} & \text{Parallel-compensated primary} \end{cases} \quad (9)$$

The imaginary part of the input impedance will be zero if the design approach in Table 2 is followed, and hence reactive power flow will be removed. In the frequency spectrum of the input impedance, there are three ZPA frequencies in general. Primary quality factor should be substantially greater than secondary quality factor to achieve a unique ZPA frequency that is

equivalent to secondary resonant frequency. The following equation defines the primary and secondary quality factors [19]

$$Q_{p,s}(\omega = \omega_0) = \frac{\mathrm{VAR}_{p,s}}{P} \tag{10}$$

where, VAR and P denotes reactive and transferred active power, respectively.

Changes in these variables might produce a phase shift in the impedance seen by the power supply in compensation networks whose primary capacitance is dependent on coupling coefficient and/or load. If the phase shift is significant, a power supply with a greater VA rating should be considered. Variable frequency control can be used to track ZPA when the coupling coefficient and/or load change. However, as previously stated, if the phase shift is considerable, the commencement of the bifurcation phenomena may result in instability and uncontrollability [20].

Although operating at ZPA frequency reduces the power supply's VA rating, it is preferable for the power supply's impedance to be somewhat inductive. The primary current will lag the inverter's output voltage in this manner, allowing for gentle switching. Soft switching causes the switches to turn on while the voltage across them is zero, thanks to an early turn on of their body diode caused by the compensation network's residual current. Zero voltage switching (ZVS) is the name for this form of soft switching. Switching loss is zero under ZVS, omitting the active switch's turn off switching loss. Turn off loss can be decreased by paralleling a capacitor (as a lossless snubber) with an active switch [21].

Because the inverter current leads the voltage, zero current switching (ZCS) can be performed if the impedance perceived from the inverter is capacitive. Since this switch is turned off when the

current crosses zero in ZCS, the turn off loss is zero. While all other switching losses (turn on loss, diode recovery loss, etc.) are retained [21], this sort of soft switching is not as useful.

The four main compensation topologies have been the subject of several studies. Three ZPA frequencies of the SS compensation network are investigated in [12]. The circuit is shown to have voltage follower characteristics at two ZPA frequencies, and current follower characteristics at the third ZPA frequency, where the compensation capacitor resonates with the self-inductance of the coils. The operating frequency is commonly set at a third of the ZPA frequency because of the high-power transmission and efficiency. Figure 4 shows the voltage gain of SS as a function of frequency fluctuations at various loads.

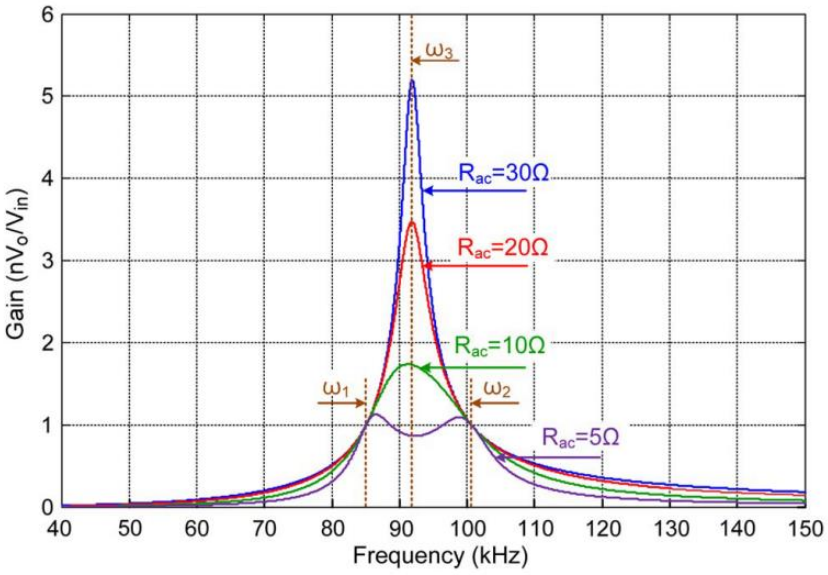

Figure 4. Voltage gain variation of a two-coil system with respect to frequency [12]

For SS and SP compensation networks, maximum efficiency and load-independent voltage transfer ratio working frequencies are examined in [21]. It is demonstrated that SS has a load-independent voltage transfer ratio at two frequencies (voltage follower frequency), whereas SP only has a load-independent voltage transfer ratio at one frequency. The operating frequency at

which SS achieves maximum transfer efficiency is deduced and referred to as ω_M. The resonant frequency of SS is proved to be close to ω_M, but its voltage follower frequency (ω_H), which is higher than resonant frequency, is far from ω_M. It is also demonstrated that operating at ω_H can result in ZVS. In SS, however, neither the resonant frequency nor ω_M have voltage follower properties. For SP compensation, on the other hand, a design approach can be used to provide optimal power transfer efficiency and voltage follower characteristics at the same frequency. Soft switching (ZVS) can be accomplished automatically for such a frequency.

[22] compares four basic compensation networks with voltage and current sources on five criteria: maximum efficiency, maximum load power transfer, load-independent output voltage and current, k-independent compensation, and no magnetic coupling allowed. The only compensation that can match all five criteria is current source SS, according to the findings. Also, except for its modest k-dependency on the maximum efficiency, current source SP compensation can match the criterion.

[23] shows that in SS compensation, if the transmitter coil's resonance frequency is too close to the working frequency, the receiver's buck converter cannot operate at high duty cycles, reducing power transfer efficiency. To avoid the region where the relationship between received power and buck converter duty cycle is inverse, a new frequency selection strategy is proposed.

Based on experimental results, [24] shows that when the load value is modest, i.e., during the constant-current stage and the beginning of the constant-voltage stage of the battery charging, SS compensation is more efficient than SP compensation. The power transfer efficiency of the SP adjustment, on the other hand, is higher for larger loads, i.e., during the constant-voltage charging stage of the battery.

Multiple modifications to the four basic compensation networks have been proposed to overcome the aforementioned problems [25], [26]. A dual topology is presented in [27] to attain constant current and constant voltage characteristics. In the secondary side, semiconductor switches are used to switch between a series-compensated and parallel-compensated configuration. [28] proposes a WPT pick up with a unity power factor that employs an LCL network as the secondary. Efficiency and cost are increased by lowering the reactive current in the secondary coil and lowering the reflected reactive power on the power supply. By adding a series capacitor, the proposed design compensates for the rectifier's effective inductive loading.

The misalignment behavior of four basic topologies is investigated and compared in [29]. SPS is a new topology that combines the properties of SS and PS compensations.

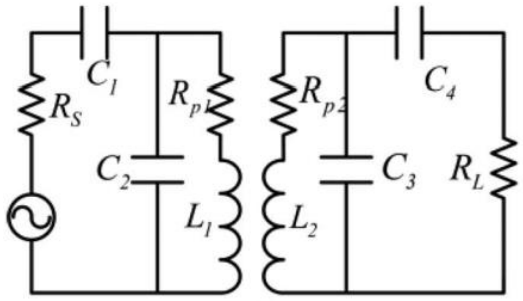

Figure 5 Mixed-resonant compensation for WPT [30]

Without any additional control loops, the suggested topology can transfer rated power with excellent efficiency in the presence of up to 25% misalignment. [30] proposes a mixed-resonant coupling circuit, as shown in Figure 5. Because it inherits the low sensitivity properties of the SS compensation, it has a better transfer efficiency than SP. The results show that if the compensation capacitors are tuned, the mixed-resonant coupling circuit exhibits constant transfer efficiency over a wide range of loads.

Two compensation systems are evaluated in [31], one with SP and the other with LCL on the primary side and a parallel capacitor on the secondary side. Although SP compensation is 2.45 percent less expensive than LCL compensation, LCL compensation achieves greater peak efficiency at rated load. Because the inverter only handles the current required to generate active power and offset the loss in the resonant tank in LCL, this is the case. In light loads, LCL is also more efficient than SP. This happens because the LCL network's input impedance rises dramatically under light loads. As a result, the inverter output current is reduced, and the conduction loss is reduced as well. SP's control complexity is also higher than LCL's due to the sensitivity of SP's reflected secondary impedance to load changes. The LCL topology boosts the secondary coil current and lowers the VA rating of resonant tank components by using partial series compensation in the primary and secondary.

A compensatory mechanism is proposed in [32] that can be used with a single transmitter and many receivers. It is also ideal for dynamic WPTs with a very dynamic receiver. The proposed structure makes use of the receiver's reflected reactance to increase the field in the coupled parts of the transmitter and receiver while weakening it in the uncoupled parts. Power transfer can be done more efficiently this manner. The electromagnetic field emissions requirement is also met without the need of elaborate shielding.

An LCC primary compensation is proposed in [17]. High order harmonics are taken into account when designing the compensating components. The voltage follower characteristic and ZCS are both included in the LCC structure. In the absence of the receiver or in the absence of a load, the input current is also limited. [33] proposes a double-sided LCC compensation network. The proposed compensation has the advantage that its resonance frequency is independent of the

coupling coefficient and load. ZVS can also be achieved for the HF inverter by tweaking the compensation network.

[26] provides a thorough examination of compensation networks. If a voltage source is employed, it is shown that the compensation network should have a T-circuit configuration to achieve a constant output voltage. -circuit arrangement should also be used to achieve constant output current with an input current source. An LC/S compensation topology is introduced in [34]. The proposed method ensures that the output current remains constant. Because there are fewer components in the LC/S architecture than in the double-sided LCC, it is more efficient and less expensive. [35] proposes an LCC compensation that is resistant to large coupling coefficient fluctuations. While the coupling coefficient fluctuates, the major goal is to achieve smooth power characteristics. Because of this, the LCC compensation is a good option for dynamic WPTs.

Control Strategies for WPT

A hybrid WPT system that charges electric vehicles at a steady proportion despite massive misalignments between charging pads is presented in [36]. To achieve a consistent and efficient charging process, the suggested charging system combines two distinct resonant networks. A mathematical model is also created that demonstrates in what manner the two resonant systems can be integrated to recompense for pad misalignment. To improve system performance under pad misalignment, [37] introduces a series-hybrid architecture where the series inductors of the main and pick-up LCL networks are merged into polarized magnetic couplers. The suggested system's behavior in misalignment is investigated using a mathematical model. Passive solutions to issues caused by coil misalignment in WPT systems, such as hybrid coil topologies [36], [37], are susceptible to power oscillations without any active control.

In [38-45], control strategies that target increased overall WPT system efficiency under coupling coefficient and/or load variations are proposed. They are mainly based on maximum efficiency tracking (or MET) methods, such as perturb and observe [40] or phase synchronization [46]. [40] begins with a thorough examination of a wireless system's efficiency at both the system and circuit levels. For peak overall system efficiency, an optimum load resistance is proven to exist in a specified mutual inductance between the transmitting and receiving coils. Then, using supplementary hardware such as a cascaded buck-boost converter, an efficiency monitoring system, and a controller, a tracking system based on perturbation and observation algorithm is designed. Without using extra hardware or establishing communication in real time between the primary side and secondary side, [46] presents a novel phase synchronization approach based on tracking the highest (or lowest, dependent on the path of the power flow) estimate of the output current. A correlation is established between the output current and the phase difference of the control indicators. The comparative phase-shift angle (time period between the center points of the primary voltage and secondary voltage) and the inner phase-shift angles (time period when the output voltage equals to the dc-link voltage) of the two converters are discovered to determine the maximum output current. Then a new control signal generation system is developed that ensures the comparative phase-shift angle is unaffected by inner phase-shift angles. After that, a process is suggested for tracking the maximum output current and obtaining the target comparative phase-shift angle for applying the phase synchronization requirement, based on the perturbation and observation method. Furthermore, considering the dead-time effect, a relationship between the transfer power and the inner phase-shift angle is derived to manage the size of the transfer power.

Some of these control strategies either require wireless communication link between primary side and secondary side [41] or eliminate the wireless link at the cost of sacrificing efficiency [42].

Others integrate MET with coupling coefficient [39] and load impedance [45] estimation methodologies. To attain the highest possible efficiency, a maximum efficiency tracking control technique is presented in [41]. As a result, the suggested WPT system satisfies both the high efficiency and constant output voltage requirements. The current of the transmitter is stored from the data obtained by the receiver through Bluetooth in the proposed control method. A charging time management method with hysteresis control of output power for the secondary-side [42] is described for WPT systems. It is a primary-side control method that combines three concepts: 1) a power flow indicator in the receiver circuit, 2) the receiver end's hysteresis switching activities of a parallel decoupling switch to manage the dc voltage level of such in-between capacitor, and 3) the decoupling switch's on and off periods are monitored on the dc voltage level of such in-between capacitor. A unique MET approach integrated with dynamic estimation of coupling coefficient is provided in [39]. This approach can accommodate practically all needs for MET, including load and coupling coefficient fluctuation adaptation, as well as output controllability. Because no new hardware or measurements are necessary, the tracking system is easy to implement. The WPT system with time-varying loads such as batteries is thoroughly investigated in [45]. A LCC compensated system with power tracking and load estimation is provided, which enables mode decision, and charging control at the primary side, as well as required load regulating and decoupling control at the receiving end. A technique of detecting coupling coefficient is also proposed and an analytical model is constructed based on the impact of reflection impedance on the inverter’s output current. For load estimation, the receiver controller supplies a reference load. The primary side controller determines battery state using an corresponding load calculation and uses dual closed-loop control to control current and power. While the charging voltage level of battery hits the limit, the receiver decouples control and sends a mode conversion signal to the

transmitter controller, which enables constant current (CC) or constant voltage (CV) mode for the battery. Because there is no data exchange between the primary and secondary sides, the Dual sides integrated control scheme can control separately, reducing the system's complexity and making it suited for various charging modes. In [44], the WPT system input impedance is extracted to operate the system with zero phase angle and consequently, to ensure optimal efficiency. Despite massive coil misalignments, this paper provides a novel control strategy that keeps the rated charging point at optimal efficiency. To compensate for inductance changes, the technique employs information collected from input impedance to regulate the system in essence at distinctive converter voltages with zero phase angle, guaranteeing that charging occurs with maximum efficiency at rated power notwithstanding pad misalignment. The essay gives a detailed analytical model that explains the hypothetical underpinnings of the suggested control viewpoint. The control methods referenced above do not guarantee stability of the WPT system.

Literature on controllers that guarantee stability of WPT system is scarce. In [43], a discrete sliding mode control (or DSMC) based design for fast MET and output voltage regulation is proposed. The adopted WPT system's power transmitter is a dc-ac inverter that uses phase angle control (based on hill-climbing-search) to achieve least input current insertion from its dc supply, resulting in least input power process. However, an additional buck-boost converter at the receiving end is required to emulate an optimum load by using the maximum energy efficiency point controlled by the DSMC based design. A Lyapunov function (or LF)-based controller for the ac-dc boost converter used for power factor correction (or PFC) in the primary side of WPT systems is proposed in [47]. The proposed controller enables the front-end PFC converter to work with fast dynamic reaction. However, the control design is not extended to the entire WPT system and is limited to the front-end power conversion stage.

Motivated by a lack of studies on stabilizing control schemes for WPT systems, an LF-based controller is projected in this thesis, which guarantees stability of the WPT system, even during the presence of load and coupling coefficient variations.

Proposed Control Strategy

WPT System with SLCC Compensation Network

Circuit Configuration

The WPT system considered in this work is depicted in Fig. 6. A secondary LCC (SLCC) compensation network provides a load-independent voltage transfer ratio and improved power transfer capability. Equivalent circuit of the SLCC compensation network and coils is shown in Figure 7.

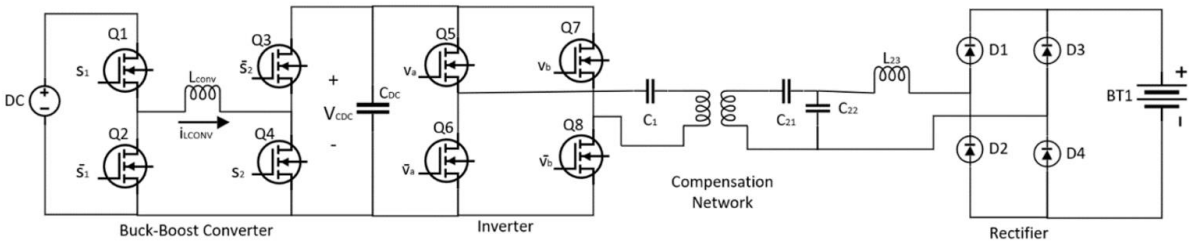

Figure 6. WPT system with SLCC compensation network

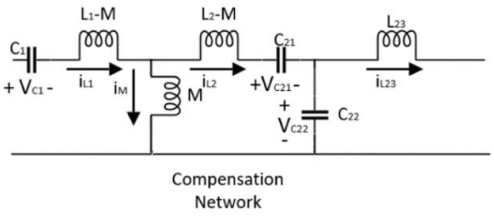

Figure 7. Equivalent circuit of the SLCC compensation network and coils

State-space Dynamic Model

The dynamics of the WPT system in Fig. 6 is expressed by the following eight differential equations, where k=0 and 1 correspond to the buck-boost converter's operation in buck and boost modes, respectively, s_1 and s_2 are duty cycles of the buck boost converter switches, and the inverter switching function is defined as $s_3 = v_a - v_b$ (see Fig. 6):

$$\frac{di_{L1}}{dt} = \frac{1}{L_1 L_2 - M^2}[L_2(s_3 v_{CDC} - v_{C1}) - M(v_{C21} + v_{C22})] \tag{11}$$

$$\frac{di_{L2}}{dt} = \frac{1}{L_1 L_2 - M^2}[M(s_3 v_{CDC} - v_{C1}) - L_1(v_{C21} + v_{C22})] \tag{12}$$

$$\frac{di_{L23}}{dt} = \frac{(v_{C22} - R i_{L23})}{L_{23}} \tag{13}$$

$$\frac{dv_{C22}}{dt} = \frac{(i_{L2} - i_{L23})}{C_{22}} \tag{14}$$

$$\frac{dv_{C1}}{dt} = \frac{i_{L1}}{C_1} \tag{15}$$

$$\frac{dv_{C21}}{dt} = \frac{i_{L2}}{C_{21}} \tag{16}$$

$$\frac{di_{LCONV}}{dt} = -\frac{[(1 - k s_2) v_{CDC} - \{k + (1 - k) s_1\} V_{in}]}{L_{CONV}} \tag{17}$$

$$\frac{dv_{CDC}}{dt} = \frac{(1 - k s_2) i_{LCONV} - s_3 i_{L1}}{C_{DC}} \tag{18}$$

Parameters used in (11)-(18) are shown in Figs. 6-7, where V_{in} is the input dc voltage in Fig. 6, and in Fig. 7, L_1, L_2 and M are self-inductances of the primary and secondary coils and mutual inductance, respectively, which are nonzero. Throughout this section, k is treated as a constant taking either the value 0 or 1, and the other model parameters are treated as positive constants, with $L_1 > M$ and $L_2 > M$.

By considering the state variables, $x_1 = i_{L1} - i_{L1}^*, x_2 = i_{L2} - i_{L2}^*, x_3 = i_{L23} - i_{L23}^*, x_4 = v_{C22} - v_{C22}^*, x_5 = v_{C1} - v_{C1}^*, \quad x_6 = v_{C21} - v_{C21}^*, x_7 = i_{LCONV} - i_{LCONV}^*, \quad x_8 = v_{CDC} - v_{CDC}^*,$ where currents and voltages with superscript "*" are the constant references with $v_{CDC}^* \neq 0$, and by defining the switching functions $s_1 = S_1 - \Delta s_1, s_2 = S_2 - \Delta s_2, s_3 = S_3 - \Delta s_3$, where $S_{1,2,3}$ and $\Delta s_{1,2,3}$ denote steady state values and small variations of $s_{1,2,3}$, respectively, the state equations of the WPT system are obtained as follows:

$$\dot{x_1} = \frac{1}{L_1 L_2 - M^2}[L_2\{(S_3 - \Delta s_3)x_8 - \Delta s_3 v_{CDC}^* - x_5\} - M(x_6 + x_4)] \tag{19}$$

$$\dot{x_2} = \frac{1}{L_1 L_2 - M^2}[M\{(S_3 - \Delta s_3)x_8 - \Delta s_3 v_{CDC}^* - x_5\} - L_1(x_6 + x_4)] \tag{20}$$

$$\dot{x_3} = \frac{x_4 - Rx_3}{L_{23}} \tag{21}$$

$$\dot{x_4} = \frac{x_2 - x_3}{C_{22}} \tag{22}$$

$$\dot{x_5} = \frac{x_1}{C_1} \tag{23}$$

$$\dot{x_6} = \frac{x_2}{C_{21}} \tag{24}$$

$$\dot{x_7} = -\frac{\{1 - k(S_2 - \Delta s_2)\}x_8 + k\Delta s_2 v_{CDC}^* + (1 - k)\Delta s_1 V_{in}}{L_{CONV}} \tag{25}$$

$$\dot{x_8} = \frac{\{1 - k(S_2 - \Delta s_2)\}x_7 + k\Delta s_2 i_{LCONV}^* - (S_3 - \Delta s_3)x_1 + \Delta s_3 i_{L1}^*}{C_{DC}} \tag{26}$$

Where the steady-state equations

$$\frac{di_{L1}^*}{dt} = \frac{1}{L_1L_2 - M^2}[L_2(S_3v_{CDC}^* - v_{C1}^*) - M(v_{C21}^* + v_{C22}^*)]$$

$$\frac{di_{L2}^*}{dt} = \frac{1}{L_1L_2 - M^2}[M(S_3v_{CDC}^* - v_{C1}^*) - L_1(v_{C21}^* + v_{C22}^*)]$$

$$\frac{di_{L23}^*}{dt} = \frac{v_{C22}^* - Ri_{L23}^*}{L_{23}}$$

$$\frac{dv_{C22}^*}{dt} = \frac{i_{L2}^* - i_{L23}^*}{C_{22}}$$

$$\frac{dv_{C1}^*}{dt} = \frac{i_{L1}^*}{C_1}$$

$$\frac{dv_{C21}^*}{dt} = \frac{i_{L2}^*}{C_{21}}$$

$$\frac{di_{LCONV}^*}{dt} = -\frac{[(1 - kS_2)v_{CDC}^* - \{k + (1 - k)S_1\}V_{in}]}{L_{CONV}}$$

$$0 = (1 - kS_2)i_{LCONV}^* - S_3i_{L1}^*$$

Relations of other reference with i_{L23}^* for constant current mode

$$v_{C22}^* = L_{23}\frac{di_{L23}^*}{dt} + Ri_{L23}^*$$

$$i_{L2}^* = i_{L23}^* + C_{22}\frac{dv_{C22}^*}{dt}$$

$$v_{C21}^* = \frac{1}{C_{21}}\int i_{L2}^*\,, \left[\frac{dv_{C21}^*}{dt} = \frac{i_{L2}^*}{C_{21}}\right]$$

$$i_{L1}^{*} = i_{M}^{*} + i_{L2}^{*} = \frac{L_2}{M} i_{L2}^{*} + \frac{1}{M}\int v_{C21}^{*} + \frac{1}{M}\int v_{C22}^{*}\,, \left[M\frac{di_{M}^{*}}{dt} = (L_2 - M)\frac{di_{L2}^{*}}{dt} + v_{C21}^{*} + v_{C22}^{*}\right]$$

$$v_{C1}^{*} = \frac{1}{C_1}\int i_{L1}^{*}$$

Lyapunov Function-Based Control Design

The Lyapunov function is selected as this energy function:

$$V(x) = \frac{1}{2}(L_1 - M){x_1}^2 + \frac{1}{2}(L_2 - M){x_2}^2 + \frac{1}{2}M(x_1 - x_2)^2 + \frac{1}{2}L_{23}{x_3}^2 + \frac{1}{2}C_{22}{x_4}^2 \quad (27)$$
$$+ \frac{1}{2}C_1{x_5}^2 + \frac{1}{2}C_{21}{x_6}^2 + \frac{1}{2}L_{CONV}{x_7}^2 + \frac{1}{2}C_{DC}{x_8}^2$$

To be a Lyapunov function for (19)-(26), (27) must satisfy the following four criteria: (i) V (0) = 0, (ii) $V(x) > 0$ if and only if $x \neq 0$, (iii) $V(x) \to \infty$ if $\|x\| \to \infty$, and (iv) $\dot{V}(x) \leq 0$ along all solutions of (9)-(16). The preceding conditions, in conjunction with the LaSalle invariance argument given in this section, will ensure global asymptotic stability (or GAS) of (19)- (26) to the origin. Clearly, (27) satisfies the first three criteria. The time derivative of (27) along (19)-(26) is obtained as follows:

$$\dot{V}(x) = (L_1 - M)x_1\dot{x_1} + (L_2 - M)x_2\dot{x_2} + M(x_1 - x_2)(\dot{x_1} - \dot{x_2}) + L_{23}x_3\dot{x_3} \quad (28)$$
$$+ C_{22}x_4\dot{x_4} + C_1x_5\dot{x_5} + C_{21}x_6\dot{x_6} + L_{CONV}x_7\dot{x_7} + C_{DC}x_8\dot{x_8}$$

After some simplification,

$$\dot{V}(x) = -R{x_3}^2 - (1-k)\Delta s_1 V_{in} x_7 - k\Delta s_2 (v^*_{CDC} x_7 - i^*_{LCONV} x_8) - \Delta s_3 (v^*_{CDC} x_1 - i^*_{L1} x_8) \quad (29)$$

For $\dot{V}(x) \leq 0$, the control components are chosen as

$$\Delta s_1 = V_{in} x_7 K_1, \;\; K_1 > 0, k = 0 \quad (30)$$

$$\Delta s_2 = (v^*_{CDC} x_7 - i^*_{LCONV} x_8) K_2, K_2 > 0, k = 1 \quad (31)$$

$$\Delta s_3 = (v^*_{CDC} x_1 - i^*_{L1} x_8) K_3, K_3 > 0 \quad (32)$$

where the K_i's are control input gains.

Therefore, stabilizing control inputs, i.e., switching functions of the buck-boost dc-dc converter and the high-frequency inverter, which satisfy these conditions and provide guaranteed stability of the system can be obtained as follows:

$$s_1 = S_1 - V_{in} K_1 (i_{LCONV} - i^*_{LCONV}), k = 0 \quad (33)$$

$$= S_1 - V_{in} K_1 x_7, k = 0$$

$$s_2 = S_2 - K_2 v^*_{CDC} i_{LCONV} + K_2 i^*_{LCONV} v_{CDC}, k = 1 \quad (34)$$

$$= S_2 - (v^*_{CDC} x_7 - i^*_{LCONV} x_8) K_2, k = 1$$

$$s_3 = S_3 - K_3 v^*_{CDC} i_{L1} + K_3 i^*_{L1} v_{CDC} \quad (35)$$

$$= S_3 - (v^*_{CDC} x_1 - i^*_{L1} x_8) K_3$$

where the reference control values S_i are given by

$$S_1 = \frac{v_{CDC}^*}{V_{in}} \tag{36}$$

$$S_2 = \frac{v_{CDC}^* - V_{in}}{v_{CDC}^*} \tag{37}$$

$$S_3 = \frac{M v_{C21}^*}{L_2 v_{CDC}^*} + \frac{v_{C1}^*}{v_{CDC}^*} \tag{38}$$

where (36) (resp., (37)) holds with k=0 (resp., k=1), because of (11) and (17) and because the structure of the dynamics (11)-(18) ensures that the appropriate reference state values must be zero.

It is assumed that $S_2 \neq 1$ and $S_3 \neq 0$ in what follows. The preceding analysis is insufficient to conclude that the preceding choices of the Δs_i's render the WPT system GAS to 0, because of the nonstrictness of V (which allows nonzero values of the state x where $\dot{V}(x) = 0$). Therefore, the well-known LaSalle invariance principle is used next to establish this GAS property, based on the fact that v_{CDC}^* is nonzero. This entails showing that any solution of the WPT system that remains in the set where $\dot{V}(x) = 0$ must be the zero solution.

To this end, two cases are considered, corresponding to the two possibilities $k = 0$ and $k = 1$ for the mode index.

Case 1: $k = 0$. In this case, the condition $\dot{V}(x) = 0$ implies that $x_3 = 0$, $x_7 = 0$, $v^*_{CDC}x_1 - i^*_{L1}x_8 = 0$, $\Delta s_3 = 0$, and $\Delta s_1 = 0$. Here and in the sequel, all equalities involving x components are for a solution of the WPT system that satisfies $\dot{V}(x) = 0$ for all $t \geq 0$. Then (21) gives $x_4 = 0$, so (22) gives $x_2 = 0$ (because $x_3 = 0$). Also, (25) gives $0 = \dot{x_7} = -x_8/L_{CONV}$, so $x_8 = 0$, so the formula $\Delta s_3 = 0$ gives $x_1 = 0$ (since $v^*_{CDC} \neq 0$). Hence, the formulas for $\dot{x_1}$ and $\dot{x_2}$ give these equations in two unknown x_5 and x_6:

$$\begin{cases} 0 = \frac{1}{a}[-L_2 x_5 - M x_6] \\ 0 = \frac{1}{a}[-M x_5 - L_1 x_6] \end{cases} \tag{39}$$

where $a = L_1 L_2 - M^2$. Since

$$det\begin{bmatrix} -L_2 & -M \\ -M & -L_1 \end{bmatrix} = a \neq 0, \tag{40}$$

it follows that $x_5 = x_6 = 0$. This gives $x = 0$.

Case 2: $k = 1$. In this case, the condition $\dot{V}(x) = 0$ implies that $x_3 = 0$,

$$v^*_{CDC}x_7 - i^*_{LCONV}x_8 = 0 \tag{41}$$

$$v^*_{CDC}x_1 - i^*_{L1}x_8 = 0 \tag{42}$$

$\Delta s_3 = 0$, and $\Delta s_2 = 0$. Then (21) gives $x_4 = 0$, so (22) gives $x_2 = 0$. Also, since (15) implies that $i_{L1}^* = 0$, and since v_{CDC}^* is nonzero, (42) implies that $x_1 = 0$. Next, note that (19) -(20) give

$$\dot{x_1} = \frac{1}{a}[L_2(S_3 x_8 - x_5) - M x_6] \tag{43}$$

$$\dot{x_2} = \frac{1}{a}[M(S_3 x_8 - x_5) - L_1 x_6] \tag{44}$$

Since $x_2 = 0$ and $M \neq 0$, (43)-(44) can be combined to get

$$\dot{x_1} = \frac{1}{a}[L_2 \frac{L_1}{M} x_6 - M x_6] = \frac{x_6}{M} \tag{45}$$

so $x_6 = 0$. Since $x_1 = x_6 = 0$, and since L_2 is nonzero, it can be concluded from (43) that $S_3 x_8 = x_5$. Since it is assumed that S_3 is nonzero, (23) therefore implies that x_5 and x_8 are constants. Since x_8 is a constant, and since $k = 1$ and $S_2 \neq 1$, (25)-(26) give $x_7 = x_8 = 0$, so it can be concluded that $x_5 = S_3 x_8 = 0$. Hence, $x = 0$ in this case as well, so the GAS property follows from the LaSalle invariance principle.

WPT System with PLCC Compensation Network

Circuit Configuration

The WPT system considered in this work is depicted in Figure 8. A primary LCC (PLCC) compensation network provides a load-independent voltage transfer ratio and improved power transfer capability. Equivalent circuit of the PLCC compensation network and coils is shown in Figure 9.

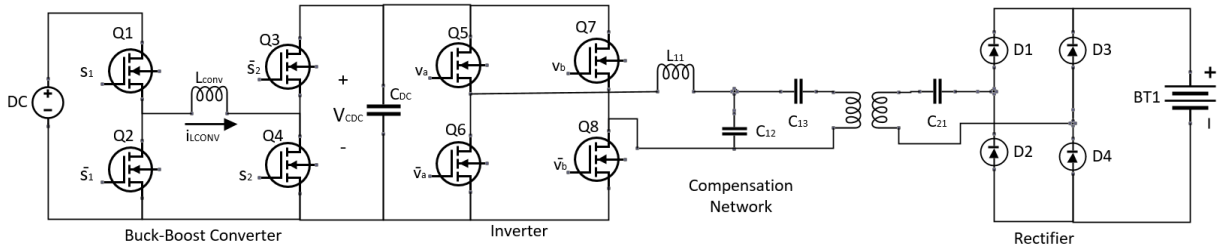

Figure 8. WPT system with PLCC compensation network

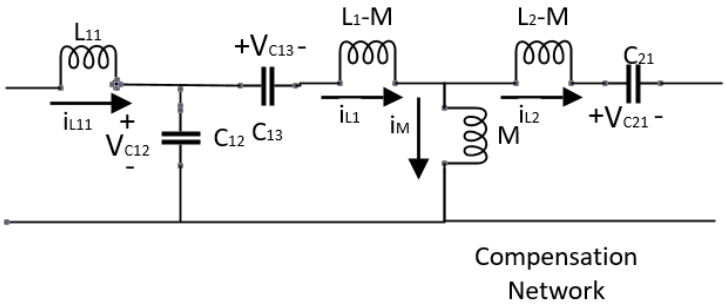

Figure 9. Equivalent circuit of the PLCC compensation network and coils

State-space Dynamic Model

The dynamics of the WPT system in Figure 8 is expressed by the following eight differential equations, where k=0 and 1 correspond to the buck-boost converter's operation in buck and boost modes, respectively, s_1 and s_2 are duty cycles of the buck boost converter switches, and the inverter switching function is defined as $s_3 = v_a - v_b$ (see Figure 8):

$$\frac{di_{L1}}{dt} = \frac{1}{L_1L_2 - M^2}\left[L_2(v_{C12} - v_{C13}) - M(v_{C21} + Ri_{L2})\right] \tag{46}$$

$$\frac{di_{L2}}{dt} = \frac{1}{L_1L_2 - M^2}\left[M(v_{C12} - v_{C13}) - L_1(v_{C21} + Ri_{L2})\right] \tag{47}$$

$$\frac{di_{L11}}{dt} = \frac{(s_3 v_{CDC} - v_{C12})}{L_{11}} \tag{48}$$

$$\frac{dv_{C12}}{dt} = \frac{(i_{L11} - i_{L1})}{C_{12}} \tag{49}$$

$$\frac{dv_{C13}}{dt} = \frac{i_{L1}}{C_{13}} \tag{50}$$

$$\frac{dv_{C21}}{dt} = \frac{i_{L2}}{C_{21}} \tag{51}$$

$$\frac{di_{LCONV}}{dt} = -\frac{[(1 - ks_2)v_{CDC} - \{k + (1-k)s_1\}V_{in}]}{L_{CONV}} \tag{52}$$

$$\frac{dv_{CDC}}{dt} = \frac{(1 - ks_2)i_{LCONV} - s_3 i_{L11}}{C_{DC}} \tag{53}$$

Parameters used in (46)-(53) are shown in Figures 8-9, where V_{in} is the input dc voltage in Fig. 1, and in Fig. 9, L_1, L_2 and M are self-inductances of the primary and secondary coils and mutual inductance, respectively, which are nonzero and similar to SLCC. Throughout this section, k is treated as a constant taking either the value 0 or 1, and the other model parameters are treated as positive constants, with $L_1 > M$ and $L_2 > M$ like SLCC.

By considering the state variables, $x_1 = i_{L1} - i_{L1}^*$, $x_2 = i_{L2} - i_{L2}^*$, $x_3 = i_{L11} - i_{L11}^*$, $x_4 = v_{C12} - v_{C12}^*$, $x_5 = v_{C13} - v_{C13}^*$, $x_6 = v_{C21} - v_{C21}^*$, $x_7 = i_{LCONV} - i_{LCONV}^*$, $x_8 = v_{CDC} - v_{CDC}^*$, where currents and voltages with superscript "*" are the constant references with $v_{CDC}^* \neq 0$, and by defining the switching functions $s_1 = S_1 - \Delta s_1$, $s_2 = S_2 - \Delta s_2$, $s_3 = S_3 - \Delta s_3$, where $S_{1,2,3}$ and

$\Delta s_{1,2,3}$ denote steady state values and small variations of $s_{1,2,3}$, respectively, the state equations of the WPT system are obtained as follows:

$$\dot{x_1} = \frac{1}{L_1 L_2 - M^2}[L_2(x_4 - x_5) - M(x_6 + Rx_2)] \tag{54}$$

$$\dot{x_2} = \frac{1}{L_1 L_2 - M^2}[M(x_4 - x_5) - L_1(x_6 + Rx_2)] \tag{55}$$

$$\dot{x_3} = \frac{(S_3 - \Delta s_3)x_8 - \Delta s_3 v_{CDC}^* - x_4}{L_{11}} \tag{56}$$

$$\dot{x_4} = \frac{x_3 - x_1}{C_{12}} \tag{57}$$

$$\dot{x_5} = \frac{x_1}{C_{13}} \tag{58}$$

$$\dot{x_6} = \frac{x_2}{C_{21}} \tag{59}$$

$$\dot{x_7} = -\frac{\{1 - k(S_2 - \Delta s_2)\}x_8 + k\Delta s_2 v_{CDC}^* + (1 - k)\Delta s_1 V_{in}}{L_{CONV}} \tag{60}$$

$$\dot{x_8} = \frac{\{1 - k(S_2 - \Delta s_2)\}x_7 + k\Delta s_2 i_{LCONV}^* - (S_3 - \Delta s_3)x_1 + \Delta s_3 i_{L11}^*}{C_{DC}} \tag{61}$$

Where the steady-state equations

$$\frac{di_{L1}^*}{dt} = \frac{1}{L_1 L_2 - M^2}[L_2(v_{C12}^* - v_{C13}^*) - M(v_{C21}^* + Ri_{L2}^*)]$$

$$\frac{di_{L2}^*}{dt} = \frac{1}{L_1 L_2 - M^2}[M(v_{C12}^* - v_{C13}^*) - L_1(v_{C21}^* + Ri_{L2}^*)]$$

$$\frac{di_{L11}^*}{dt} = \frac{S_3 v_{CDC}^* - v_{C12}^*}{L_{11}}$$

$$\frac{dv_{C12}^*}{dt} = \frac{i_{L11}^* - i_{L1}^*}{C_{12}}$$

$$\frac{dv_{C13}^*}{dt} = \frac{i_{L1}^*}{C_{13}}$$

$$\frac{dv_{C21}^*}{dt} = \frac{i_{L2}^*}{C_{21}}$$

$$\frac{di_{LCONV}^*}{dt} = -\frac{[(1-kS_2)v_{CDC}^* - \{k+(1-k)S_1\}V_{in}]}{L_{CONV}}$$

$$0 = (1-kS_2)i_{LCONV}^* - S_3 i_{L11}^*$$

Relations of other reference with i_{L2}^* for constant current mode

$$v_{C21}^* = \frac{1}{C_{21}}\int i_{L2}^* \,, \left[\frac{dv_{C21}^*}{dt} = \frac{i_{L2}^*}{C_{21}}\right]$$

$$i_{L1}^* = i_M^* + i_{L2}^* = \frac{L_2}{M} i_{L2}^* + \frac{1}{M}\int v_{C21}^* + \frac{R}{M}\int i_{L2}^* \,, \left[M\frac{di_M^*}{dt} = (L_2 - M)\frac{di_{L2}^*}{dt} + v_{C21}^* + Ri_{L2}^*\right]$$

$$v_{C13}^* = \frac{1}{C_{13}}\int i_{L1}^*$$

$$v_{C12}^* = v_{C13}^* + (L_1 - M)\frac{di_{L1}^*}{dt} + (L_2 - M)\frac{di_{L2}^*}{dt} + v_{C21}^* + Ri_{L2}^*$$

$$i_{L11}^* = i_{L1}^* + C_{12}\frac{dv_{C12}^*}{dt}$$

Lyapunov Function-Based Control Design

The Lyapunov function is selected as this energy function:

$$V(x) = \frac{1}{2}(L_1 - M){x_1}^2 + \frac{1}{2}(L_2 - M){x_2}^2 + \frac{1}{2}M(x_1 - x_2)^2 + \frac{1}{2}L_{11}{x_3}^2 + \frac{1}{2}C_{12}{x_4}^2 \quad (62)$$
$$+ \frac{1}{2}C_{13}{x_5}^2 + \frac{1}{2}C_{21}{x_6}^2 + \frac{1}{2}L_{CONV}{x_7}^2 + \frac{1}{2}C_{DC}{x_8}^2$$

To be a Lyapunov function for (54)-(61), (62) must satisfy the following four criteria: (i) $V(0) = 0$, (ii) $V(x) > 0$ if and only if $x \neq 0$, (iii) $V(x) \to \infty$ if $\|x\| \to \infty$, and (iv) $\dot{V}(x) \leq 0$ along all solutions of (54)-(61). The preceding conditions, in conjunction with the LaSalle invariance argument given in this section, will ensure global asymptotic stability (or GAS) of (54)-(61) to the origin. Clearly, (62) satisfies the first three criteria. The time derivative of (62) along (54)-(61) is obtained as follows:

$$\dot{V}(x) = (L_1 - M)x_1\dot{x_1} + (L_2 - M)x_2\dot{x_2} + M(x_1 - x_2)(\dot{x_1} - \dot{x_2}) + L_{11}x_3\dot{x_3} \quad (63)$$
$$+ C_{12}x_4\dot{x_4} + C_{13}x_5\dot{x_5} + C_{21}x_6\dot{x_6} + L_{CONV}x_7\dot{x_7} + C_{DC}x_8\dot{x_8}$$

After some simplification,

$$\dot{V}(x) = -R{x_2}^2 - (1 - k)\Delta s_1 V_{in}x_7 - k\Delta s_2(v_{CDC}^* x_7 - i_{LCONV}^* x_8) - \Delta s_3(v_{CDC}^* x_3 \quad (64)$$
$$- i_{L11}^* x_8)$$

For $\dot{V}(x) \leq 0$, the control components are chosen as

$$\Delta s_1 = V_{in}x_7K_1, K_1 > 0, k = 0 \quad (65)$$

$$\Delta s_2 = (v_{CDC}^* x_7 - i_{LCONV}^* x_8) K_2, K_2 > 0, k = 1 \tag{66}$$

$$\Delta s_3 = (v_{CDC}^* x_3 - i_{L11}^* x_8) K_3, K_3 > 0 \tag{67}$$

where the K_i's are control input gains.

Therefore, stabilizing control inputs, i.e., switching functions of the buck-boost dc-dc converter and the high-frequency inverter, which satisfy these conditions and provide guaranteed stability of the system can be obtained as follows:

$$s_1 = S_1 - V_{in} K_1 (i_{LCONV} - i_{LCONV}^*), k = 0 \tag{68}$$

$$= S_1 - V_{in} K_1 x_7, k = 0$$

$$s_2 = S_2 - K_2 v_{CDC}^* i_{LCONV} + K_2 i_{LCONV}^* v_{CDC}, k = 1 \tag{69}$$

$$= S_2 - (v_{CDC}^* x_7 - i_{LCONV}^* x_8) K_2, k = 1$$

$$s_3 = S_3 - K_3 v_{CDC}^* i_{L11} + K_3 i_{L11}^* v_{CDC} \tag{70}$$

$$= S_3 - (v_{CDC}^* x_3 - i_{L11}^* x_8) K_3$$

where the reference control values S_i are given by

$$S_1 = \frac{v_{CDC}^*}{V_{in}} \tag{71}$$

$$S_2 = \frac{v_{CDC}^* - V_{in}}{v_{CDC}^*} \tag{72}$$

$$S_3 = \frac{v_{C1}^*}{v_{CDC}^*} \tag{73}$$

where (71) (resp., (72)) holds with k=0 (resp., k=1), because of (46) and (52) and because the structure of the dynamics (46)-(53) ensures that the appropriate reference state values must be zero.

It is assumed that $S_2 \neq 1$ and $S_3 \neq 0$ in what follows. The preceding analysis is insufficient to conclude that the preceding choices of the Δs_i's render the WPT system GAS to 0, because of the nonstrictness of V (which allows nonzero values of the state x where $\dot{V}(x) = 0$). Therefore, the well-known LaSalle invariance principle is used next to establish this GAS property, based on the fact that v_{CDC}^* is nonzero. This entails showing that any solution of the WPT system that remains in the set where $\dot{V}(x) = 0$ must be the zero solution.

To this end, two cases are considered, corresponding to the two possibilities $k = 0$ and $k = 1$ for the mode index.

Case 1: $k = 0$. In this case, the condition $\dot{V}(x) = 0$ implies that $x_2 = 0$, $x_7 = 0$, $v_{CDC}^* x_3 - i_{L11}^* x_8 = 0$, $\Delta s_3 = 0$, and $\Delta s_1 = 0$.

Here and in the sequel, all equalities involving x components are for a solution of the WPT system that satisfies $\dot{V}(x)=0$ for all $t \geq 0$. Then (60) gives $x_8 = 0$, so (61) gives $x_3 = 0$ (because $x_7 = 0$). Also, (56) gives $0 = \dot{x_7} = -x_4/L_{11}$, so $x_4 = 0$ and (57) gives $x_1=0$. Hence, the formulas for $\dot{x_1}$ and $\dot{x_2}$ give these equations in two unknown x_5 and x_6:

$$\begin{cases} 0 = \frac{1}{a}[-L_2 x_5 - M x_6] \\ 0 = \frac{1}{a}[-M x_5 - L_1 x_6] \end{cases} \tag{74}$$

where $a = L_1 L_2 - M^2$. Since

$$det\begin{bmatrix} -L_2 & -M \\ -M & -L_1 \end{bmatrix} = a \neq 0, \tag{75}$$

it follows that $x_5 = x_6 = 0$. This gives $x = 0$.

Case 2: $k = 1$. In this case, the condition $\dot{V}(x)$=0 implies that $x_2 = 0$,

$$v_{CDC}^* x_7 - i_{LCONV}^* x_8 = 0 \tag{76}$$

$$v_{CDC}^* x_3 - i_{L11}^* x_8 = 0 \tag{77}$$

$\Delta s_3 = 0$, and $\Delta s_2 = 0$. (55) and (56) give

$$\dot{x_1} = \frac{1}{a}[L_2(x_4 - x_5) - M x_6] \tag{78}$$

$$0 = M(x_4 - x_5) - L_1 x_6 \tag{79}$$

Since $M \neq 0$, (78)-(79) can be combined to get

$$\dot{x_1} = \frac{1}{a}\left[L_2 \frac{L_1}{M} x_6 - M x_6\right] = \frac{x_6}{M} \tag{80}$$

(59) gives $\dot{x_6}$ = 0 and it follows that $\dot{x_4} = \dot{x_5}$ using (69). Hence, (47) and (48) give

$$x_3 = \frac{C_{12} + C_{13}}{C_{13}} x_1 = a x_1 \tag{81}$$

(76) and (77) gives

$$-v^*_{CDC} \frac{(1 - S_2) x_8}{L_{CONV}} = i^*_{LCONV} \frac{(1 - S_2) x_7 - S_3 x_1}{C_{DC}} \tag{82}$$

$$v^*_{CDC} \frac{S_3 x_8 - x_4}{L_{11}} = i^*_{L11} \frac{(1 - S_2) x_7 - S_3 x_1}{C_{DC}} \tag{83}$$

(82) and (83) gives

$$x_4 = \left[S_3 + \frac{i^*_{L11} L_{11}}{i^*_{LCONV} L_{CONV}} (1 - S_2)\right] x_8 = b x_8 = b \frac{v^*_{CDC}}{i^*_{L11}} x_3 = c x_3 = b \frac{v^*_{CDC}}{i^*_{LCONV}} x_7 \tag{84}$$

$$= d x_7$$

(81), (82) and (84) give that $x_1 = x_3 = x_4 = x_7 = x_8 = 0$. (80) gives $x_6 = 0$ and hence (79) gives $x_5 = 0$.

Results And Discussions

WPT System with SLCC Compensation Network

The parameters of the WPT system are listed in Table 3. The coil and compensation network parameters are obtained following the design procedure proposed in [48]. The control input gains are set to $K_1 = -5e^{-6}$, $K_2 = -5e^{-6}$ and $K_3 = -10e^{-6}$ to satisfy the stability criteria. The dc-link voltage reference, v_{CDC}^{*}, is set to 240 V. When transmitter and receiver coils are fully aligned, the coupling coefficient is 0.22.

Table 3. WPT system parameters

Parameter [unit]	Value
$f_{sw\text{-}inv}$ [kHz]	80
k [-]	0.22
R [Ω]	11.5, 67.5
V_{in} [V]	180
V_{out} [V]	110
C_{DC} [mF]	6
C_f [µF]	0.22
L_f [µH]	240
L_{conv} [µH]	240
L_1 [µH]	253
L_2 [µH]	249
L_{23}	38.5
L_{11}	76.5
C_{12} [nF]	51.7
C_{13} [nF]	21.7
C_{21} [nF] for PLCC	15.9
C_1 [nF]	15.6
C_{22} [nF]	103
C_{21} [nF] for SLCC	18.3

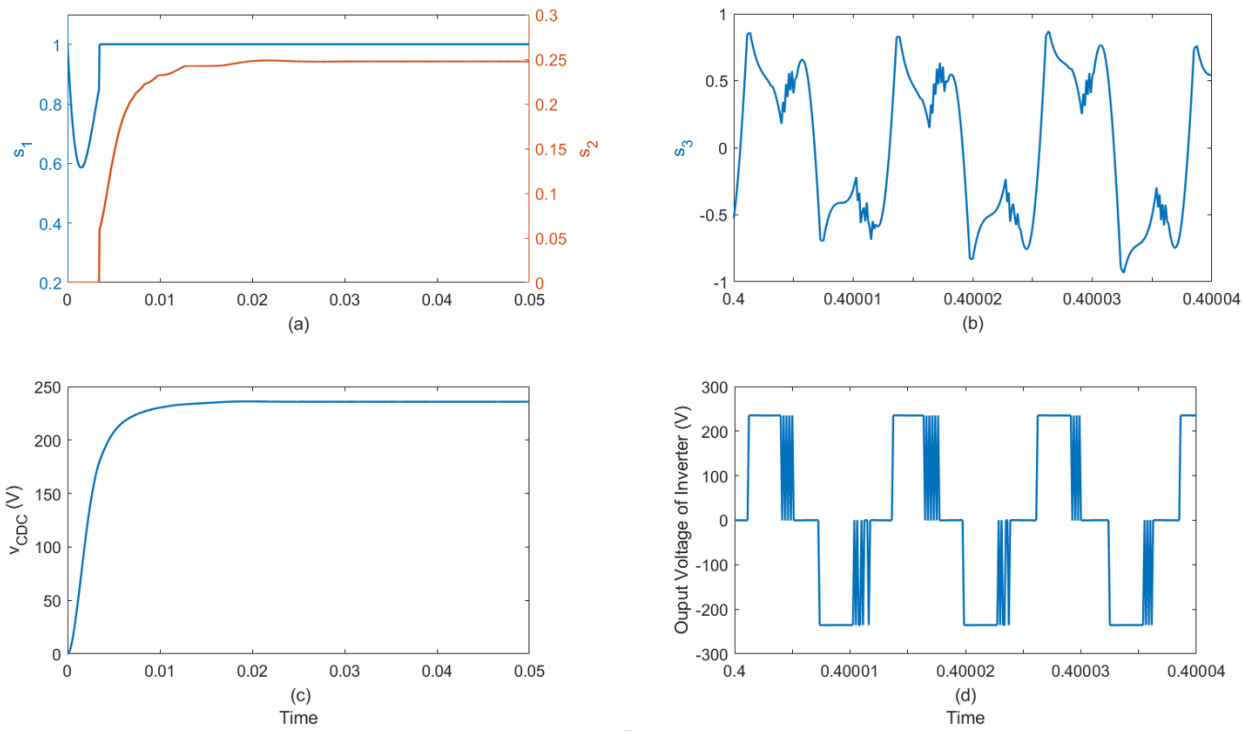

Figure 10 (a) Switching Functions $s1$ and $s2$ which control the Buck-Boost Converter, (b) Switching Function $s3$ which controls the inverter, (c) Output voltage of the Buck-Boost Converter $vCDC$ and (d) Output voltage of the inverter in the WPT system for Lyapunov Function Based Controller

The battery, which is modeled as a variable resistance, is charged in constant current (CC) mode followed by the constant voltage (CV) mode. The control is not active at the beginning until v_{CDC} reaches the level of input voltage (Figure 10 (c)). The switching functions s_1 and s_2 control the buck-boost converter (Figure 10 (a)) and the switching function s_3 controls the high frequency inverter (Figure 10 (b)). The switching function s_3 is initiated when the output voltage of buck-boost converter reaches a certain level.

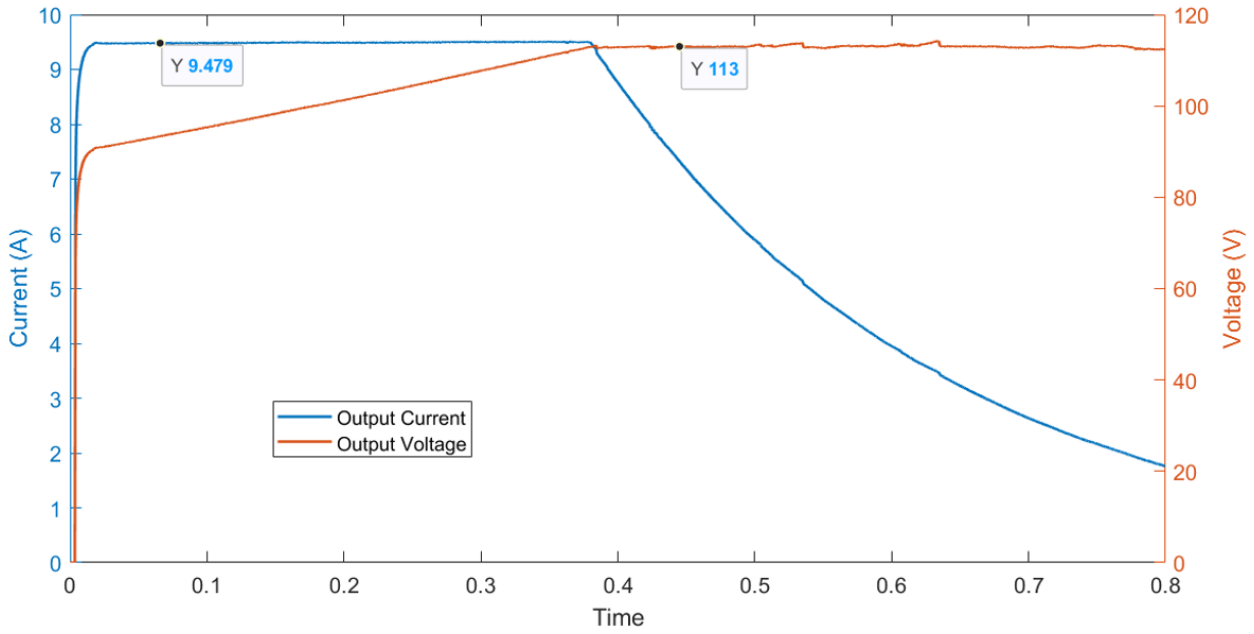

Figure 11. Output Voltage and Current of the WPT system for Lyapunov Function Based Controller for Constant Current Mode followed by Constant Voltage Mode

As seen in Figure 11, in the CC mode, the battery current is maintained at ~9.5 A by appropriately adjusting i_{L23}^{*}. The battery voltage is maintained at ~113 V in CV mode by appropriately adjusting v_{C22}^{*}. These reference values are obtained using charge/discharge characteristics of a 2.5 kWh Li-Ion battery in the lab. The remaining reference state variables are obtained using the equations provided earlier. Figures 12 and 13 depict the reference and actual current of LCC network inductors and the reference and actual current of LCC network capacitors voltages. Figures 12 and 13 also contains the zoomed version to show how the actual current or voltage is following the reference current or voltage. As it can be seen, all control variables follow their respective references. Figure 14 illustrates all eight state variables, x_1, …, x_8, of the system that converge to zero.

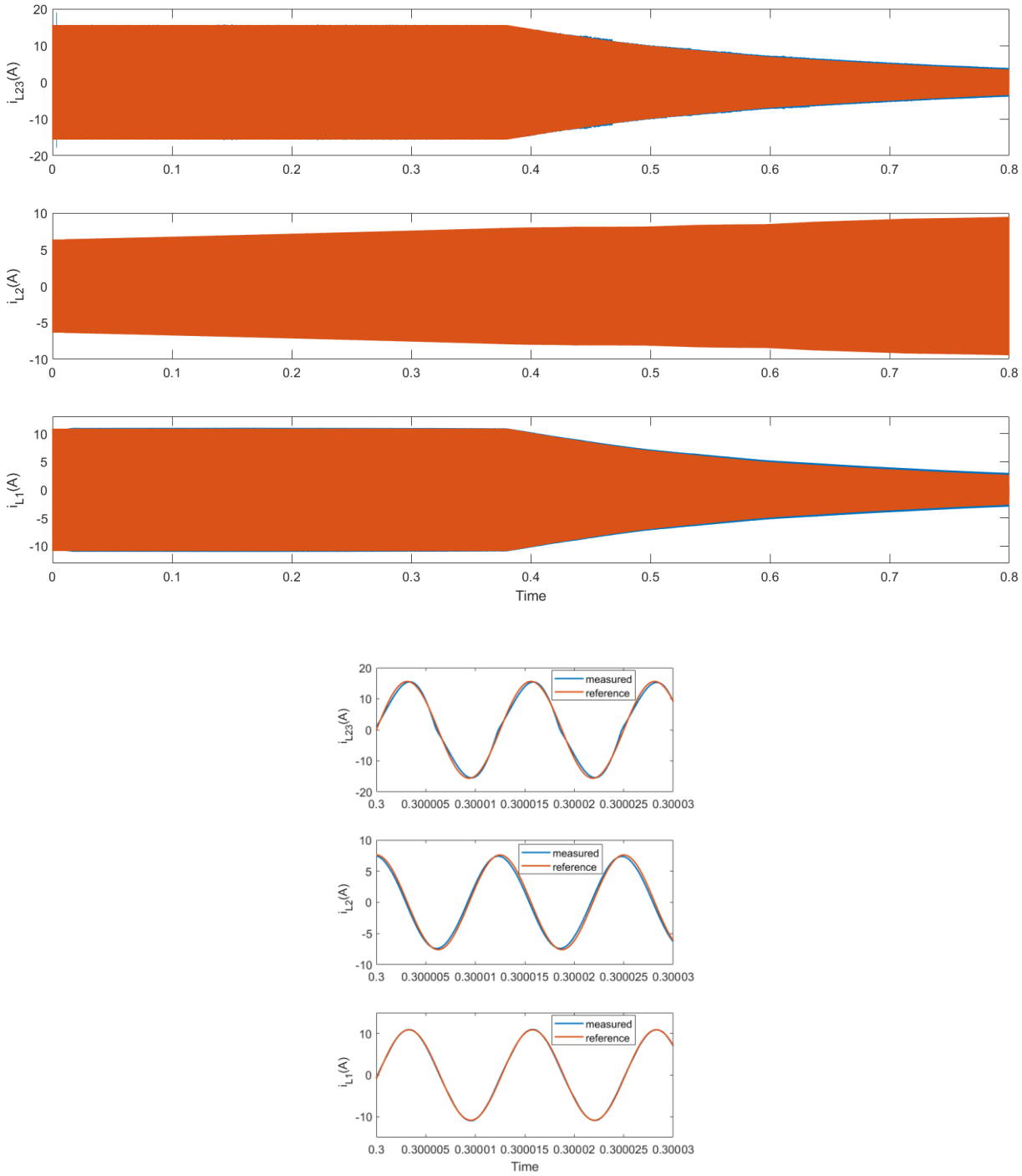

Figure 12. The reference and actual current of SLCC Compensation Network inductors for Lyapunov Function Based Controller for Constant Current Mode followed by Constant Voltage Mode

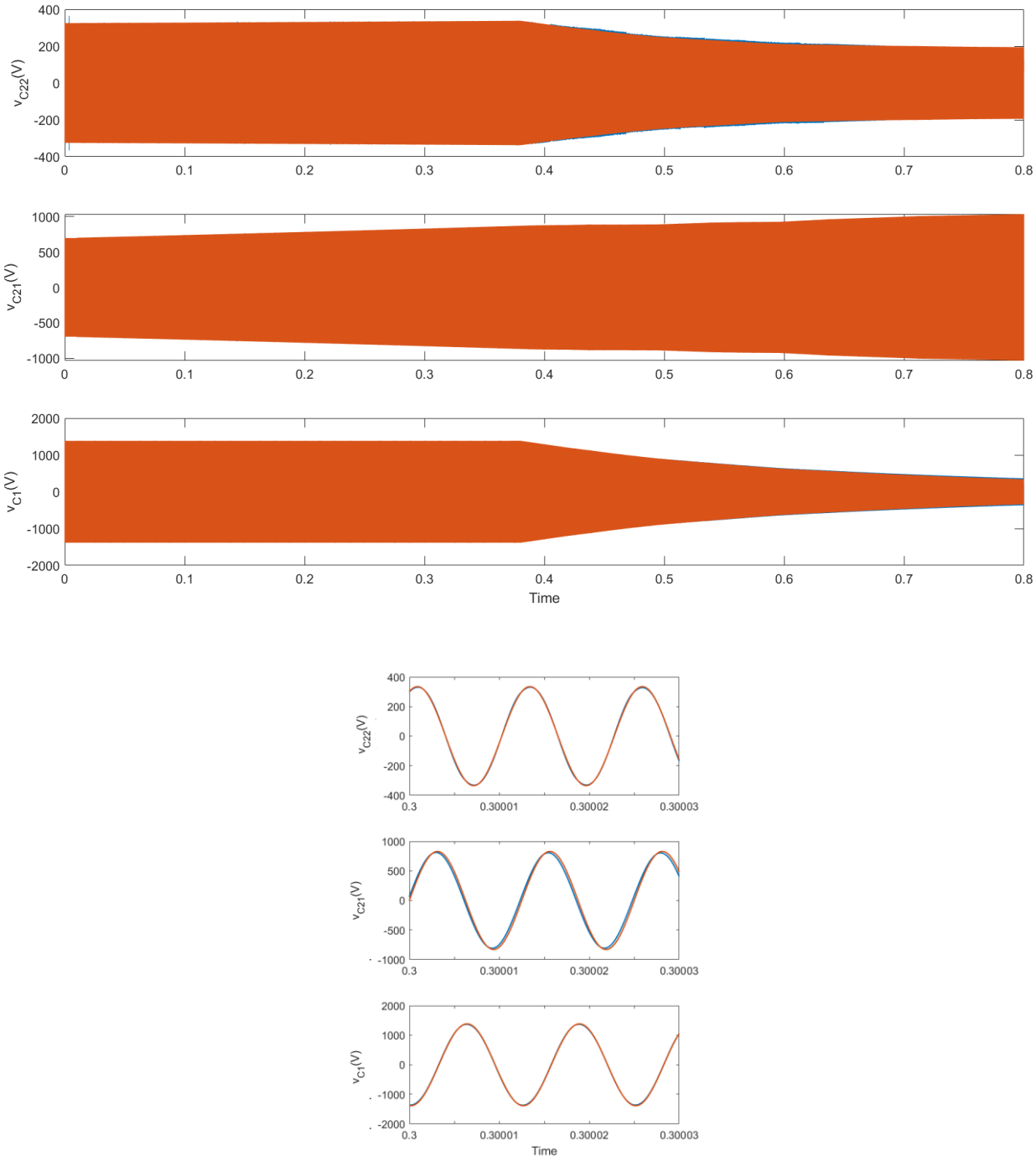

Figure 13. The reference and actual voltages the of SLCC Compensation Network capacitors for Lyapunov Function Based Controller for Constant Current Mode followed by Constant Voltage Mode

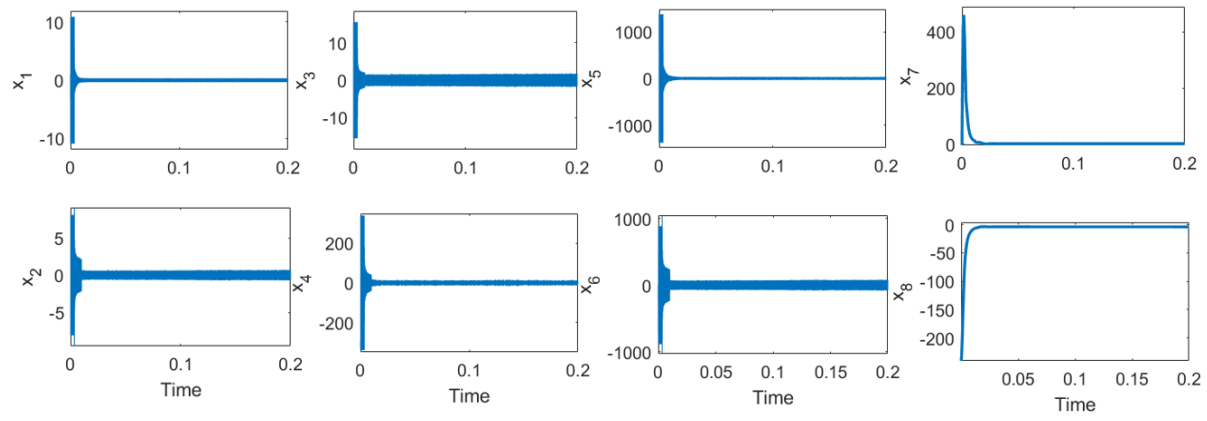

Figure 14. State Variables of Lyapunov Controller for the SLCC Compensation Network based WPT system in Constant Current Mode with k=0.22

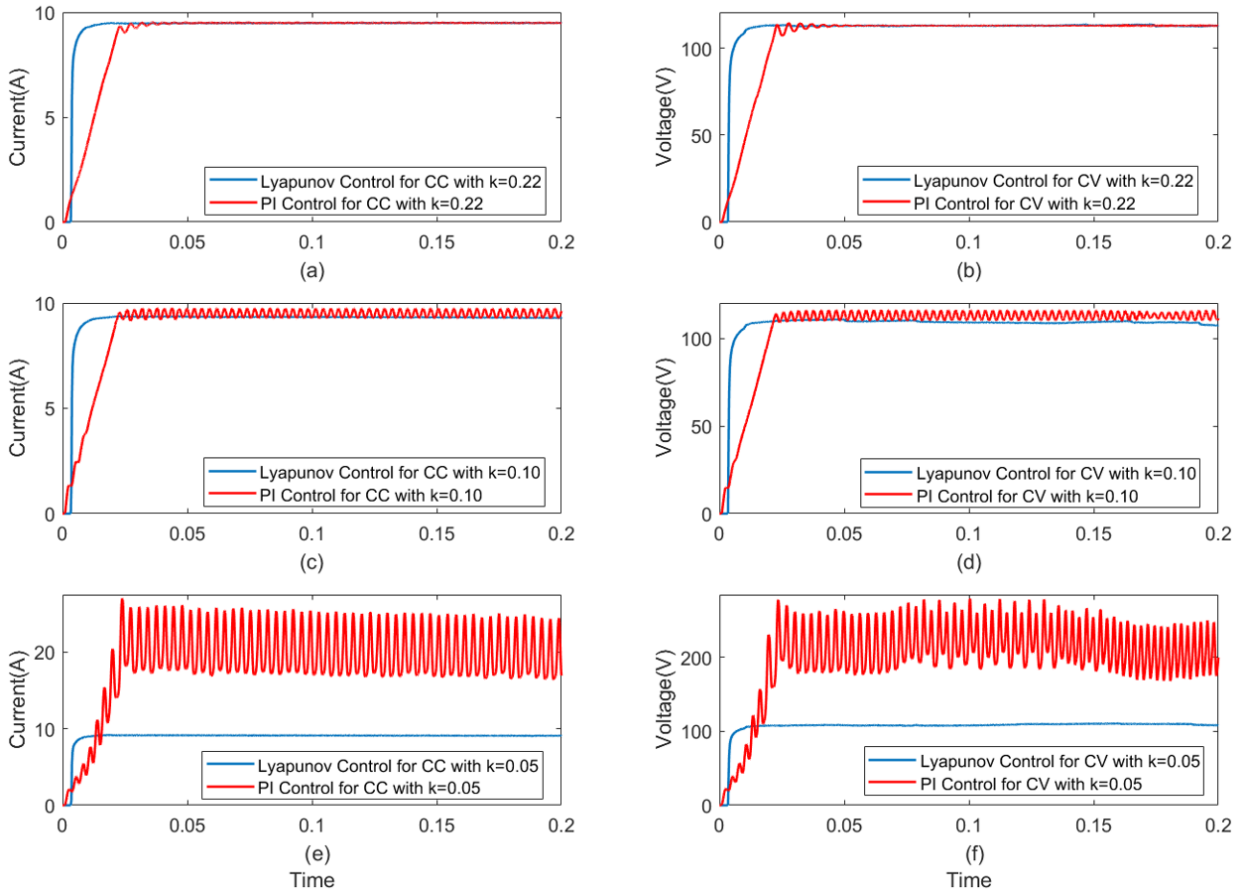

Figure 15. Output Voltage of the WPT system for Lyapunov Controller and PI Controller in Constant Current (CC) Mode (a, c, e) and Constant Voltage (CV) Mode (b, d, f) for different coupling coefficient (k=0.22, 0.10 and 0.05)

This illustrates how the proposed LF-based controller is able to restrain dynamics of the system around an equilibrium, resulting in asymptotic stability of the WPT system, even under varying output load.

As another case study, performance of the proposed LF-based controller and a conventional PI-based controller is evaluated and compared when primary and secondary coils are misaligned. In these studies, the variable resistance load is charged in CC and CV modes separately. Figure 15 illustrates the results for coupling coefficient of 0.22 (no misalignment), 0.1 (misalignment level 1) and 0.05 (misalignment level 2). It is seen that in both CC and CV modes, the LF-based controller maintains stability of the system even under acute misalignment (misalignment level 2) of the primary and secondary coils, whereas the PI-based controller becomes unstable.

WPT System with PLCC Compensation Network

The parameters of the WPT system are listed in Table 3. The coil and compensation network parameters are obtained following the design procedure proposed in [48]. The control input gains are set to $K_1 = -5e^{-6}$, $K_2 = -5e^{-6}$ and $K_3 = -10e^{-6}$ to satisfy the stability criteria. The dc-link voltage reference, v_{CDC}^{*}, is set to 240 V. When transmitter and receiver coils are fully aligned, the coupling coefficient is 0.22.

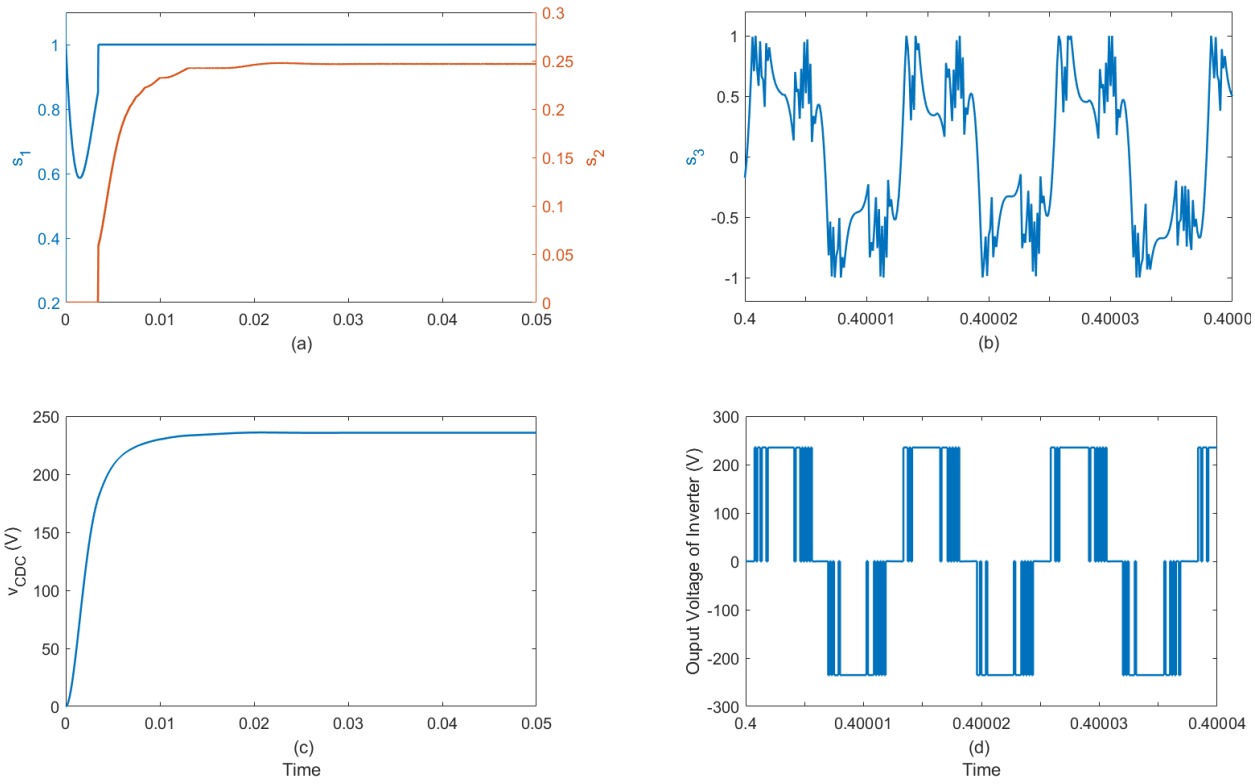

Figure 16. (a) Switching Functions s_1 and s_2 which control the Buck-Boost Converter, (b) Switching Function s_3 which controls the inverter, (c) Output voltage of the Buck-Boost Converter v_{CDC} and (d) Output voltage of the inverter in the PLCC Compensation Network based WPT system for Lyapunov Function Based Controller.

The battery, which is modeled as a variable resistance, is charged in constant current (CC) mode followed by the constant voltage (CV) mode. The control is not active at the beginning until v_{CDC} reaches the level of input voltage (Figure 166 (c)). The switching functions s_1 and s_2 control the buck-boost converter (Figure 16 (a)) and the switching function s_3 controls the high frequency inverter (Figure 16 (b)). The switching function s_3 is initiated when the output voltage of buck-boost converter reaches a certain level.

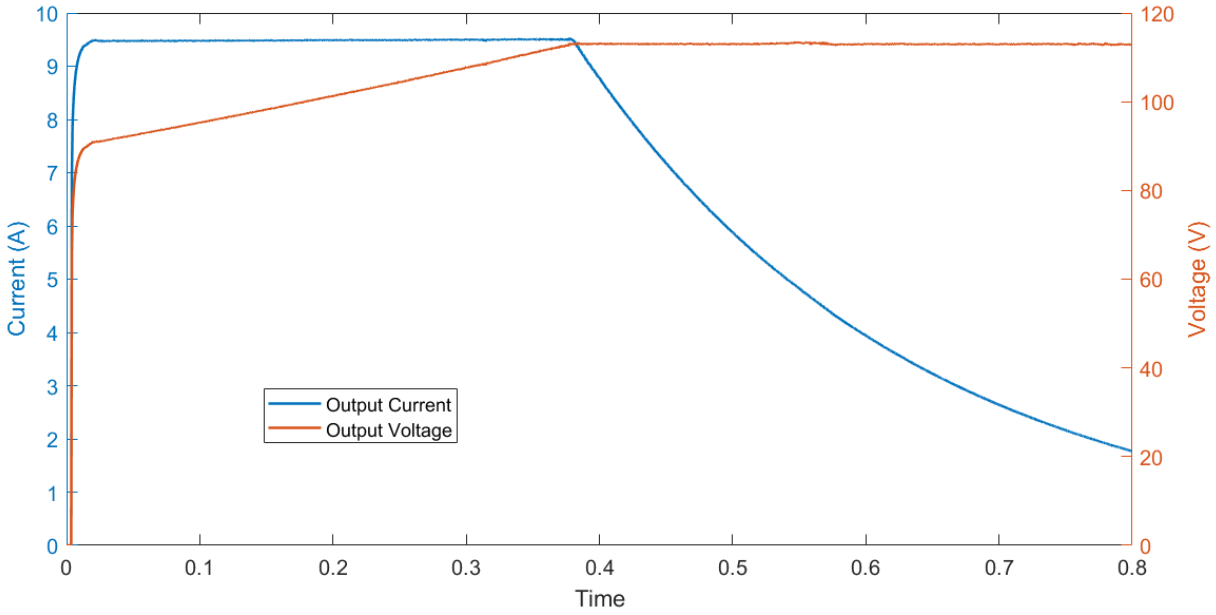

Figure 17. Output Voltage and Current of the PLCC Compensation Network based WPT system for Lyapunov Function Based Controller for Constant Current Mode followed by Constant Voltage Mode

As seen in Figure 17, in the CC mode, the battery current is maintained at ~9.5 A by appropriately adjusting i_{L2}^{*}. These reference values are obtained using charge/discharge characteristics of a 2.5 kWh Li-Ion battery in the lab. The remaining reference state variables are obtained using the equations provided earlier. Figures 18 and 19 depict the reference and actual current of LCC network inductors and the reference and actual current of LCC network capacitors voltages. As it can be seen, all control variables follow their respective references. Fig. 19 illustrates all eight state variables, x_1, …, x_8, of the system that converge to zero.

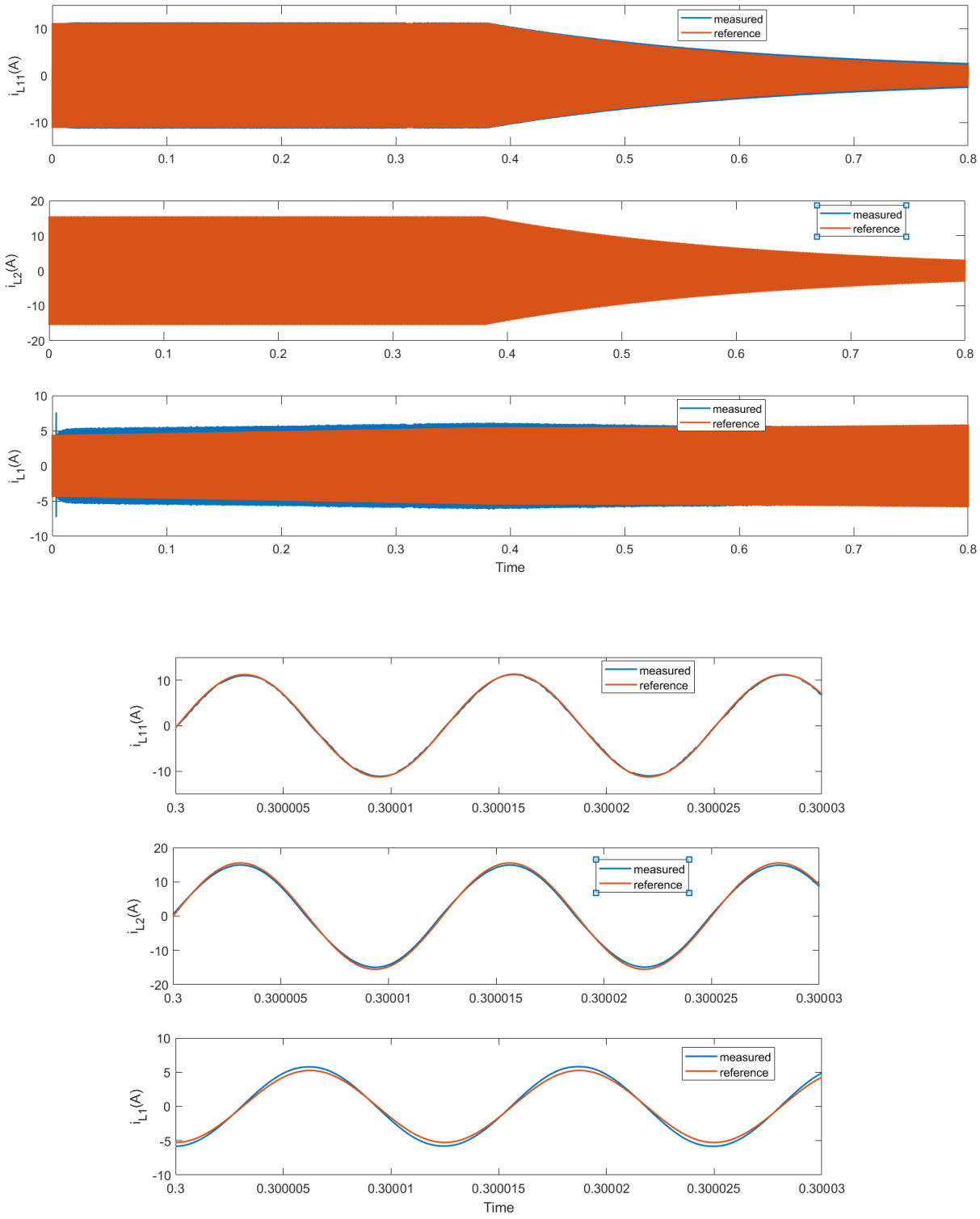

Figure 18. The reference and actual currents the of PLCC Compensation Network inductors for Lyapunov Function Based Controller for Constant Current Mode followed by Constant Voltage Mode

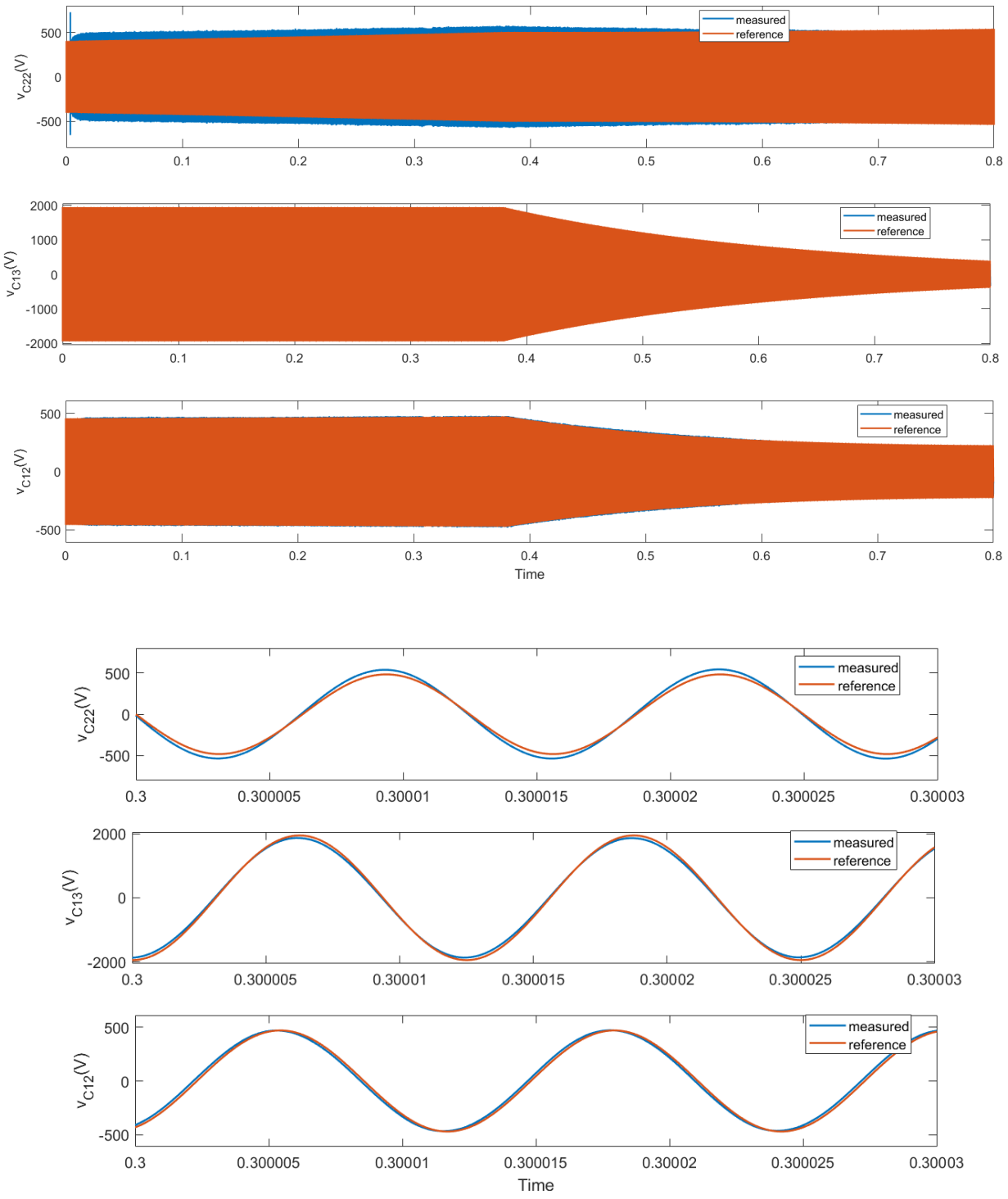

Figure 19. The reference and actual voltages the of PLCC Compensation Network capacitors for Lyapunov Function Based Controller for Constant Current Mode followed by Constant Voltage Mode

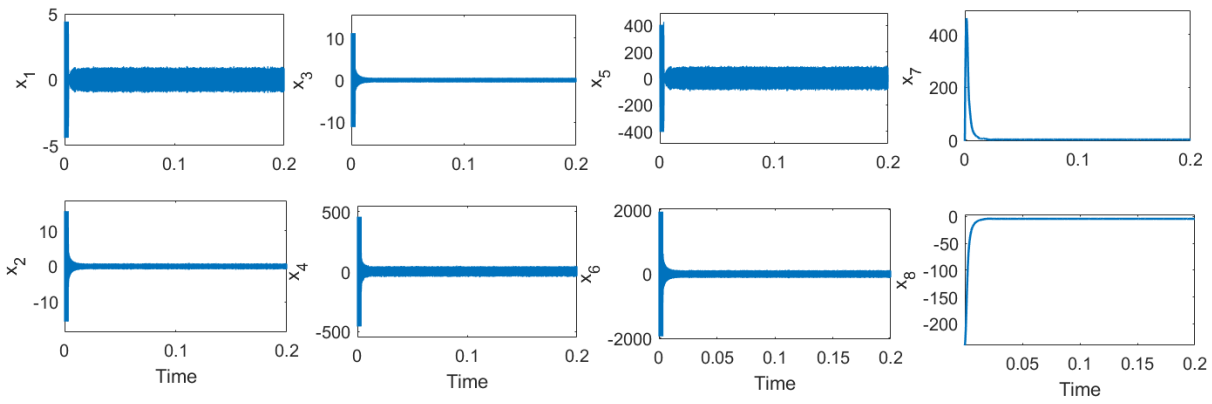

Figure 20. State Variables of Lyapunov Controller for the PLCC Compensation Network based WPT system in Constant Current Mode with k=0.22

This illustrates how the proposed LF-based controller is able to restrain dynamics of the system around an equilibrium, resulting in asymptotic stability of the WPT system, even under varying output load.

Future Work

The following activities are recommended for further work

- To develop a method for estimating coupling coefficient. Coupling coefficient estimation is a very significant step for this method because coupling coefficient changes with misalignment.
- To develop a state estimator to obtain internal impedance of the battery.
- To implement the Controller in the WPT setup. FPGA based fast controllers should be selected to implement the Lyapunov based Controller.

Conclusion

Motivated by a lack of studies on stabilizing control schemes for WPT systems, a novel LF-based scheme is proposed. The proposed controller guarantees GAS of the WPT system. This was shown using a LaSalle invariance argument, which is valid in both the buck and boost modes of operation. Comparative studies with a PI-based controller show effectiveness of the proposed controller in maintaining the stability of the WPT system, even under the load and coupling coefficient variations. Prototyping a 1.2 kW WPT system in the lab is recently finalized. The setup will be used to evaluate performance of the proposed controller with a battery load and under misalignment of the transmitter and receiver coils.

References

[1] W. Li, H. Zhao, J. Deng, S. Li, and C. C. Mi, "Comparison Study on SS and Double-Sided LCC Compensation Topologies for EV/PHEV Wireless Chargers," *IEEE Transactions on Vehicular Technology*, vol. 65, no. 6, pp. 4429-4439, 2016, doi: 10.1109/TVT.2015.2479938.

[2] D. Patil, M. K. McDonough, J. M. Miller, B. Fahimi, and P. T. Balsara, "Wireless Power Transfer for Vehicular Applications: Overview and Challenges," *IEEE Transactions on Transportation Electrification*, vol. 4, no. 1, pp. 3-37, 2018, doi: 10.1109/TTE.2017.2780627.

[3] A. K. RamRakhyani, S. Mirabbasi, and M. Chiao, "Design and Optimization of Resonance-Based Efficient Wireless Power Delivery Systems for Biomedical Implants," *IEEE Transactions on Biomedical Circuits and Systems*, vol. 5, no. 1, pp. 48-63, 2011, doi: 10.1109/TBCAS.2010.2072782.

[4] L. Ó, L. A. Barragán, J. M. Burdio, J. Ó, D. Navarro, and I. Urriza, "A Versatile Power Electronics Test-Bench Architecture Applied to Domestic Induction Heating," *IEEE Transactions on Industrial Electronics*, vol. 58, no. 3, pp. 998-1007, 2011, doi: 10.1109/TIE.2010.2048840.

[5] J. Yungtaek and M. M. Jovanovic, "A contactless electrical energy transmission system for portable-telephone battery chargers," *IEEE Transactions on Industrial Electronics*, vol. 50, no. 3, pp. 520-527, 2003, doi: 10.1109/TIE.2003.812472.

[6] H. Z. Z. Beh, G. A. Covic, and J. T. Boys, "Investigation of Magnetic Couplers in Bicycle Kickstands for Wireless Charging of Electric Bicycles," *IEEE Journal of Emerging and Selected Topics in Power Electronics*, vol. 3, no. 1, pp. 87-100, 2015, doi: 10.1109/JESTPE.2014.2325866.

[7] M. Ibrahim *et al.*, "Inductive Charger for Electric Vehicle: Advanced Modeling and Interoperability Analysis," *IEEE Transactions on Power Electronics*, vol. 31, no. 12, pp. 8096-8114, 2016, doi: 10.1109/TPEL.2016.2516344.

[8] R. Tavakoli, A. Jovicic, N. Chandrappa, R. Bohm, and Z. Pantic, "Design of a dual-loop controller for in-motion wireless charging of an electric bus," in *2016 IEEE Energy Conversion Congress and Exposition (ECCE)*, 18-22 Sept. 2016 2016, pp. 1-8, doi: 10.1109/ECCE.2016.7855021.

[9] L. Seokhwan *et al.*, "The optimal design of high-powered power supply modules for wireless power transferred train," in *2012 Electrical Systems for Aircraft, Railway and Ship Propulsion*, 16-18 Oct. 2012 2012, pp. 1-4, doi: 10.1109/ESARS.2012.6387396.

[10] N. Shinohara, "Power without wires," *IEEE Microwave Magazine*, vol. 12, no. 7, pp. S64-S73, 2011, doi: 10.1109/MMM.2011.942732.

[11] W. X. Zhong, X. Liu, and S. Y. R. Hui, "A Novel Single-Layer Winding Array and Receiver Coil Structure for Contactless Battery Charging Systems With Free-Positioning and Localized Charging Features," *IEEE Transactions on Industrial Electronics,* vol. 58, no. 9, pp. 4136-4144, 2011, doi: 10.1109/TIE.2010.2098379.

[12] S. Moon, B. Kim, S. Cho, C. Ahn, and G. Moon, "Analysis and Design of a Wireless Power Transfer System With an Intermediate Coil for High Efficiency," *IEEE Transactions on Industrial Electronics,* vol. 61, no. 11, pp. 5861-5870, 2014, doi: 10.1109/TIE.2014.2301762.

[13] S. Li and C. C. Mi, "Wireless Power Transfer for Electric Vehicle Applications," *IEEE Journal of Emerging and Selected Topics in Power Electronics,* vol. 3, no. 1, pp. 4-17, 2015, doi: 10.1109/JESTPE.2014.2319453.

[14] R. Severns, E. Yeow, G. Woody, J. Hall, and J. Hayes, "An ultra-compact transformer for a 100 W to 120 kW inductive coupler for electric vehicle battery charging," in *Proceedings of Applied Power Electronics Conference. APEC '96,* 3-7 March 1996 1996, vol. 1, pp. 32-38 vol.1, doi: 10.1109/APEC.1996.500418.

[15] K. W. Klontz, D. M. Divan, and D. W. Novotny, "An actively cooled 120 kW coaxial winding transformer for fast charging electric vehicles," *IEEE Transactions on Industry Applications,* vol. 31, no. 6, pp. 1257-1263, 1995, doi: 10.1109/28.475695.

[16] A. P. Sample, D. T. Meyer, and J. R. Smith, "Analysis, Experimental Results, and Range Adaptation of Magnetically Coupled Resonators for Wireless Power Transfer," *IEEE Transactions on Industrial Electronics,* vol. 58, no. 2, pp. 544-554, 2011, doi: 10.1109/TIE.2010.2046002.

[17] Z. Pantic, S. Bai, and S. M. Lukic, "ZCS LCC-Compensated Resonant Inverter for Inductive-Power-Transfer Application," *IEEE Transactions on Industrial Electronics,* vol. 58, no. 8, pp. 3500-3510, 2011, doi: 10.1109/TIE.2010.2081954.

[18] W. Zhang, S. Wong, C. K. Tse, and Q. Chen, "Design for Efficiency Optimization and Voltage Controllability of Series–Series Compensated Inductive Power Transfer Systems," *IEEE Transactions on Power Electronics,* vol. 29, no. 1, pp. 191-200, 2014, doi: 10.1109/TPEL.2013.2249112.

[19] W. Chwei-Sen, G. A. Covic, and O. H. Stielau, "Power transfer capability and bifurcation phenomena of loosely coupled inductive power transfer systems," *IEEE Transactions on Industrial Electronics,* vol. 51, no. 1, pp. 148-157, 2004, doi: 10.1109/TIE.2003.822038.

[20] W. Chwei-Sen, O. H. Stielau, and G. A. Covic, "Design considerations for a contactless electric vehicle battery charger," *IEEE Transactions on Industrial Electronics,* vol. 52, no. 5, pp. 1308-1314, 2005, doi: 10.1109/TIE.2005.855672.

[21] W. Zhang, S. Wong, C. K. Tse, and Q. Chen, "Analysis and Comparison of Secondary Series- and Parallel-Compensated Inductive Power Transfer Systems Operating for Optimal Efficiency and Load-Independent Voltage-Transfer Ratio," *IEEE Transactions on Power Electronics,* vol. 29, no. 6, pp. 2979-2990, 2014, doi: 10.1109/TPEL.2013.2273364.

[22] Y. H. Sohn, B. H. Choi, E. S. Lee, G. C. Lim, G. Cho, and C. T. Rim, "General Unified Analyses of Two-Capacitor Inductive Power Transfer Systems: Equivalence of Current-Source SS and SP Compensations," *IEEE Transactions on Power Electronics,* vol. 30, no. 11, pp. 6030-6045, 2015, doi: 10.1109/TPEL.2015.2409734.

[23] D. Ahn, "Transmitter Coil Resonant Frequency Selection for Wireless Power Transfer," *IEEE Transactions on Power Electronics,* vol. 33, no. 6, pp. 5029-5041, 2018, doi: 10.1109/TPEL.2017.2730924.

[24] G. Buja, M. Bertoluzzo, and K. N. Mude, "Design and Experimentation of WPT Charger for Electric City Car," *IEEE Transactions on Industrial Electronics,* vol. 62, no. 12, pp. 7436-7447, 2015, doi: 10.1109/TIE.2015.2455524.

[25] X. Dai *et al.*, "Improved LCL resonant network for Inductive Power Transfer system," in *2015 IEEE PELS Workshop on Emerging Technologies: Wireless Power (2015 WoW)*, 5-6 June 2015 2015, pp. 1-5, doi: 10.1109/WoW.2015.7132844.

[26] W. Zhang and C. C. Mi, "Compensation Topologies of High-Power Wireless Power Transfer Systems," *IEEE Transactions on Vehicular Technology,* vol. 65, no. 6, pp. 4768-4778, 2016, doi: 10.1109/TVT.2015.2454292.

[27] C. Auvigne, P. Germano, D. Ladas, and Y. Perriard, "A dual-topology ICPT applied to an electric vehicle battery charger," in *2012 XXth International Conference on Electrical Machines*, 2-5 Sept. 2012 2012, pp. 2287-2292, doi: 10.1109/ICElMach.2012.6350201.

[28] N. A. Keeling, G. A. Covic, and J. T. Boys, "A Unity-Power-Factor IPT Pickup for High-Power Applications," *IEEE Transactions on Industrial Electronics,* vol. 57, no. 2, pp. 744-751, 2010, doi: 10.1109/TIE.2009.2027255.

[29] J. L. Villa, J. Sallan, J. F. S. Osorio, and A. Llombart, "High-Misalignment Tolerant Compensation Topology For ICPT Systems," *IEEE Transactions on Industrial Electronics,* vol. 59, no. 2, pp. 945-951, 2012, doi: 10.1109/TIE.2011.2161055.

[30] L. Chen, S. Liu, Y. C. Zhou, and T. J. Cui, "An Optimizable Circuit Structure for High-Efficiency Wireless Power Transfer," *IEEE Transactions on Industrial Electronics,* vol. 60, no. 1, pp. 339-349, 2013, doi: 10.1109/TIE.2011.2179275.

[31] B. Esteban, M. Sid-Ahmed, and N. C. Kar, "A Comparative Study of Power Supply Architectures in Wireless EV Charging Systems," *IEEE Transactions on Power Electronics,* vol. 30, no. 11, pp. 6408-6422, 2015, doi: 10.1109/TPEL.2015.2440256.

[32] K. Lee, Z. Pantic, and S. M. Lukic, "Reflexive Field Containment in Dynamic Inductive Power Transfer Systems," *IEEE Transactions on Power Electronics,* vol. 29, no. 9, pp. 4592-4602, 2014, doi: 10.1109/TPEL.2013.2287262.

[33] S. Li, W. Li, J. Deng, T. D. Nguyen, and C. C. Mi, "A Double-Sided LCC Compensation Network and Its Tuning Method for Wireless Power Transfer," *IEEE Transactions on Vehicular Technology,* vol. 64, no. 6, pp. 2261-2273, 2015, doi: 10.1109/TVT.2014.2347006.

[34] Y. Wang, Y. Yao, X. Liu, D. Xu, and L. Cai, "An LC/S Compensation Topology and Coil Design Technique for Wireless Power Transfer," *IEEE Transactions on Power Electronics,* vol. 33, no. 3, pp. 2007-2025, 2018, doi: 10.1109/TPEL.2017.2698002.

[35] H. Feng, T. Cai, S. Duan, J. Zhao, X. Zhang, and C. Chen, "An LCC-Compensated Resonant Converter Optimized for Robust Reaction to Large Coupling Variation in Dynamic Wireless Power Transfer," *IEEE Transactions on Industrial Electronics,* vol. 63, no. 10, pp. 6591-6601, 2016, doi: 10.1109/TIE.2016.2589922.

[36] L. Zhao, D. J. Thrimawithana, and U. K. Madawala, "Hybrid Bidirectional Wireless EV Charging System Tolerant to Pad Misalignment," *IEEE Transactions on Industrial Electronics,* vol. 64, no. 9, pp. 7079-7086, 2017, doi: 10.1109/TIE.2017.2686301.

[37] L. Zhao, D. J. Thrimawithana, U. K. Madawala, A. P. Hu, and C. C. Mi, "A Misalignment-Tolerant Series-Hybrid Wireless EV Charging System With Integrated Magnetics," *IEEE Transactions on Power Electronics,* vol. 34, no. 2, pp. 1276-1285, 2019, doi: 10.1109/TPEL.2018.2828841.

[38] T. Diekhans and R. W. D. Doncker, "A Dual-Side Controlled Inductive Power Transfer System Optimized for Large Coupling Factor Variations and Partial Load," *IEEE Transactions on Power Electronics,* vol. 30, no. 11, pp. 6320-6328, 2015, doi: 10.1109/TPEL.2015.2393912.

[39] X. Dai, X. Li, Y. Li, and A. P. Hu, "Maximum Efficiency Tracking for Wireless Power Transfer Systems With Dynamic Coupling Coefficient Estimation," *IEEE Transactions on Power Electronics,* vol. 33, no. 6, pp. 5005-5015, 2018, doi: 10.1109/TPEL.2017.2729083.

[40] M. Fu, H. Yin, X. Zhu, and C. Ma, "Analysis and Tracking of Optimal Load in Wireless Power Transfer Systems," *IEEE Transactions on Power Electronics,* vol. 30, no. 7, pp. 3952-3963, 2015, doi: 10.1109/TPEL.2014.2347071.

[41] T. Yeo, D. Kwon, S. Khang, and J. Yu, "Design of Maximum Efficiency Tracking Control Scheme for Closed-Loop Wireless Power Charging System Employing Series Resonant Tank," *IEEE Transactions on Power Electronics,* vol. 32, no. 1, pp. 471-478, 2017, doi: 10.1109/TPEL.2016.2523121.

[42] W. Zhong and S. Y. R. Hui, "Charging Time Control of Wireless Power Transfer Systems Without Using Mutual Coupling Information and Wireless Communication System," *IEEE Transactions on Industrial Electronics,* vol. 64, no. 1, pp. 228-235, 2017, doi: 10.1109/TIE.2016.2598725.

[43] Y. Yang, W. Zhong, S. Kiratipongvoot, S. Tan, and S. Y. R. Hui, "Dynamic Improvement of Series–Series Compensated Wireless Power Transfer Systems Using Discrete Sliding Mode Control," *IEEE Transactions on Power Electronics,* vol. 33, no. 7, pp. 6351-6360, 2018, doi: 10.1109/TPEL.2017.2747139.

[44] Y. Liu, U. K. Madawala, R. Mai, and Z. He, "Zero-Phase-Angle Controlled Bidirectional Wireless EV Charging Systems for Large Coil Misalignments," *IEEE Transactions on Power Electronics,* vol. 35, no. 5, pp. 5343-5353, 2020, doi: 10.1109/TPEL.2019.2941709.

[45] Q. Zhao, A. Wang, J. Liu, and X. Wang, "The Load Estimation and Power Tracking Integrated Control Strategy for Dual-Sides Controlled LCC Compensated Wireless Charging System," *IEEE Access,* vol. 7, pp. 75749-75761, 2019, doi: 10.1109/ACCESS.2019.2922329.

[46] F. Liu, K. Li, K. Chen, and Z. Zhao, "A Phase Synchronization Technique Based on Perturbation and Observation for Bidirectional Wireless Power Transfer System," *IEEE Journal of Emerging and Selected Topics in Power Electronics,* vol. 8, no. 2, pp. 1287-1297, 2020, doi: 10.1109/JESTPE.2019.2942101.

[47] M. Pahlevaninezhad, P. Das, J. Drobnik, G. Moschopoulos, P. K. Jain, and A. Bakhshai, "A Nonlinear Optimal Control Approach Based on the Control-Lyapunov Function for an AC/DC Converter Used in Electric Vehicles," *IEEE Transactions on Industrial Informatics,* vol. 8, no. 3, pp. 596-614, 2012, doi: 10.1109/TII.2012.2193894.

[48] A. M. Bozorgi and M. Farasat, "Wireless Power Transfer Coil Design for Transmitter and Receiver LCC Compensation based on Time-Weighted Average Efficiency," in *2019 IEEE Applied Power Electronics Conference and Exposition (APEC)*, 17-21 March 2019 2019, pp. 3100-3106, doi: 10.1109/APEC.2019.8722045.

Vita

Abu Shahir Md Khalid Hasan was born in Rangpur, Bangladesh in 1991 to Abul Kalam Azad and Shahan Ara Begum. He completed SCC and HSC from Dhaka Residential Model College. He has completed MSc in BUET on ‘Design of A One-Way Communication Based Control Scheme for Power Management Unit in Scalable DC Microgrid Architecture’ which is an effort to provide reliable renewable energy for deprived people of Bangladesh in the remote regions. He has published 3 IEEE conference paper and 1 IEEJ journal paper during this period. His undergraduate thesis was on ‘Elastography Imaging using Ultrasound Backscattered Radio Frequency Data in the Frequency Domain’ which was effort to detect cancer more precisely. He even published 1 IEEE conference paper during his undergraduate study.

Abu Shahir Md Khalid Hasan is a very active member in the lab and worked numerous projects during his undergraduate studies. Power Factor Improvement (PFI) System, Multi-meter with USB interfacing and VLSI Chip design of 9-bit parity checker are some of his projects which can be mentioned in this regard. Being in top-9 among 50 teams from all over Bangladesh in the competition "Global Robotics Challenge: Bangladesh Round 2013 shows his interest and passion real life electrical challenges.

After his graduation, Abu Shahir Md Khalid Hasan got an offer of academic position in the Dept. of EEE, Daffodil International University, Bangladesh, where he is involved in various projects and thesis supervision. Currently he is working in the Green Energy and Transportation Systems (GRENT) lab in LSU, to build controller for wireless charger of electric vehicles.